

A large topographic feature on the surface of the trans-Neptunian object (307261) 2002 MS₄ measured from stellar occultations[★]

F. L. Rommel^{1,2,3}, F. Braga-Ribas^{3,1,2}, J. L. Ortiz⁴, B. Sicardy⁵, P. Santos-Sanz⁴, J. Desmars^{6,7}, J. I. B. Camargo^{1,2}, R. Vieira-Martins^{1,2}, M. Assafin^{8,2}, B. E. Morgado^{8,2,1}, R. C. Bouffeur^{1,2}, G. Benedetti-Rossi^{9,5,2}, A. R. Gomes-Júnior^{10,9,2}, E. Fernández-Valenzuela¹¹, B. J. Holler¹², D. Souami^{5,13,14**}, R. Duffard⁴, G. Margoti^{3,2}, M. Vara-Lubiano⁴, J. Lecacheux⁵, J. L. Plouvier¹⁵, N. Morales⁴, A. Maury¹⁶, J. Fabrega¹⁷, P. Ceravolo¹⁸, E. Jehin¹⁹, D. Albanese²⁰, H. Marley²¹, S. Cikota^{22,23}, D. Ruždjak²⁴, A. Cikota²⁵, R. Szakáts^{26,27}, D. Baba Aissa²⁸, Z. Gringahcene²⁸, V. Kashuba²⁹, N. Koshkin²⁹, V. Zhukov³⁰, S. Fişek^{31,32}, O. Çakır^{33,34}, S. Özer^{35,36}, C. Schnabel^{37,38}, M. Schnabel³⁸, F. Signoret³⁹, L. Morrone^{40,41}, T. Santana-Ros^{42,43}, C. L. Pereira^{1,2,3}, M. Emilio^{44,1,3}, A. Y. Burdanov⁴⁵, J. de Wit⁴⁵, K. Barkaoui^{46,45,47}, M. Gillon⁴⁶, G. Leto⁴⁸, A. Frasca⁴⁸, G. Catanzaro⁴⁸, R. Zanmar Sanchez⁴⁸, U. Tagliaferri⁴⁹, M. Di Sora⁴⁹, G. Isopi⁴⁹, Y. Krugly^{50,51}, I. Slyusarev⁵⁰, V. Chiorny⁵⁰, H. Mikuž^{52,53}, P. Bacci⁵⁴, M. Maestriperi⁵⁴, M. D. Grazia⁵⁴, I. de la Cueva⁵⁵, M. Yuste-Moreno⁵⁵, F. Ciabattari⁵⁶, O. M. Kozhukhov⁵⁷, M. Serra-Ricart^{47,58}, M. R. Alarcon^{47,58}, J. Licandro^{47,58}, G. Masi⁵⁹, R. Bacci⁶⁰, J. M. Bosch⁶¹, R. Behem⁶², J.-P. Prost⁶², S. Renner^{7,63}, M. Conjat²¹, M. Bachini⁶⁴, G. Succi⁶⁴, L. Stoian⁶⁵, A. Juravle⁶⁵, D. Carosati⁶⁶, B. Gowe⁶⁷, J. Carrillo⁶⁸, A. P. Zheleznyak⁵⁰, N. Montigiani⁶⁹, C. R. Foster⁷⁰, M. Mannucci⁶⁹, N. Ruocco⁷¹, F. Cuevas⁷², P. Di Marcantonio⁷³, I. Coretti⁷³, G. Iafrate⁷³, V. Baldini⁷³, M. Collins⁷⁴, A. Pál²⁶, B. Csák²⁶, E. Fernández-García⁴, A. J. Castro-Tirado⁴, L. Hudin⁷⁵, J. M. Madiedo⁴, R. M. Anghel⁷⁶, J. F. Calvo-Fernández⁷⁷, A. Valvasori^{78,79}, E. Guido⁸⁰, R. M. Gherase⁸¹, S. Kamoun^{82,83}, R. Fafet⁶², M. Sánchez-González^{84,85}, L. Curelaru⁸⁶, C. D. Vîntdevară⁸⁷, C. A. Danescu⁸⁸, J.-F. Gout⁸⁹, C. J. Schmitz⁹⁰, A. Sota⁴, I. Belskaya^{5,50}, M. Rodríguez-Marco⁹¹, Y. Kilic^{92,93}, E. Frappa⁹⁴, A. Klotz⁹⁵, M. Lavayssière⁹⁶, J. Marques Oliveira⁵, M. Popescu⁸⁸, L. A. Mammama^{97,98}, E. Fernández-Lajús^{98,99}, M. Schmidt¹⁰⁰, U. Hopp¹⁰⁰, R. Komžík¹⁰¹, T. Pribulla¹⁰¹, D. Tomko¹⁰¹, M. Husárik¹⁰¹, O. Erece^{93,92}, S. Eryilmaz⁹³, L. Buzzi¹⁰², B. Gährken¹⁰³, D. Nardiello^{104,105}, K. Hornoch¹⁰⁶, E. Sonbas^{107,108}, H. Er¹⁰⁹, V. Burwitz¹¹⁰, P. Waldemar Sybilski¹¹¹, W. Bykowski¹¹¹, T. G. Müller¹¹⁰, W. Ogloza¹¹², R. Gonçalves¹¹³, J. F. Ferreira¹¹⁴, M. Ferreira¹¹⁵, M. Bento¹¹⁵, S. Meister^{116,117}, M. N. Bagiran¹¹⁸, M. Tekeş^{119,120}, A. Marciniak⁵¹, Z. Moravec¹²¹, P. Delinčák¹²², G. Gianni¹²³, G. B. Casalnuovo¹²⁴, M. Boutet¹²⁵, J. Sanchez¹²⁶, B. Klemt^{37,127}, N. Wuensche³⁷, W. Burzynski^{128,129,37}, M. Borkowski¹³⁰, M. Serrau¹³¹, G. Dangi³⁷, O. Klös³⁷, C. Weber³⁷, M. Urbaník¹³², L. Rousselot¹³¹, J. Kubánek^{37,133,134}, P. Andre¹³⁵, C. Colazo^{136,137,138}, J. Spagnotto¹³⁹, A. A. Sickafoose¹⁴⁰, R. Hueso¹⁴¹, A. Sánchez-Lavega¹⁴¹, R. S. Fisher¹⁴², A. W. Rengstorf¹⁴³, C. Perelló^{38,37}, M. Dascalu¹⁴⁴, M. Altan¹⁴⁵, K. Gazeas¹⁴⁶, T. de Santana^{5,9,147}, R. Sfair^{9,147}, O. C. Winter⁹, S. Kalkan¹⁴⁸, O. Canales-Moreno³⁸, J. M. Trigo-Rodríguez¹⁴⁹, V. Tsamis¹⁵⁰, K. Tigani¹⁵⁰, N. Sioulas¹⁵¹, G. Lekkas¹⁵², D. N. Bertesteanu⁸¹, V. Dumitrescu¹⁵³, A. J. Wilberger¹⁵⁴, J. W. Barnes¹⁵⁵, S. K. Fieber-Beyer¹⁵⁶, R. L. Swaney¹⁵⁷, C. Fuentes^{158,159,160}, R. A. Mendez¹⁵⁸, B. D. Dumitru¹⁶¹, R. L. Flynn¹⁶², and D. A. Wake¹⁶³

(Affiliations can be found after the references)

Last version: August 24, 2023

ABSTRACT

Context. The physical characterization of trans-Neptunian objects is essential for improving our understanding of the formation and evolution of our Solar System. Stellar occultation is a ground-based technique that can be successfully used to determine some of the TNOs' fundamental physical properties with high precision, such as size and shape.

Aims. This work is aimed at constraining the size, shape, and geometric albedo of the dwarf planet candidate (307261) 2002 MS₄ through the analysis of nine stellar occultation events. Using multichord detection, we also study the object's topography by analyzing the obtained limb and residuals between the observed chords and the best-fit ellipse.

Methods. We predicted and organized the observational campaigns of nine stellar occultations by 2002 MS₄ between 2019 and 2022, resulting in two single-chord events, four double-chord detections, and three events with between 3 and 61 positive chords. We derived the occultation light curves using differential aperture photometry, from which the star ingress and egress instants were calculated. Using 13 selected chords from the 8 August 2020 event, we determined the global elliptical limb of 2002 MS₄. The best-fit ellipse, combined with the object's rotational information from the literature, sets constraints on the object's size, shape, and albedo. Additionally, we developed a new method to characterize the topography features on the object's limb.

Results. The global limb has a semi-major axis of $a' = 412 \pm 10$ km, a semi-minor axis of $b' = 385 \pm 17$ km, and the position angle of the minor axis is $121^\circ \pm 16^\circ$. From this instantaneous limb, we obtained 2002 MS₄'s geometric albedo of $p_V = 0.1 \pm 0.025$, using $H_V = 3.63 \pm 0.05$ mag and a projected area-equivalent diameter of 796 ± 24 km. Significant deviations from the fitted ellipse in the northernmost limb were detected from multiple sites, highlighting three distinct topographic features: one 11 km depth depression, followed by a 25^{+4}_{-5} km height elevation next to a crater-like depression, with an extension of 322 ± 39 km and 45.1 ± 1.5 km deep.

Conclusions. Our results indicate the presence of an object that is ≈ 138 km smaller in diameter than that derived from thermal data, possibly indicating the presence of a thus-far unknown satellite. However, within the error bars, the geometric albedo in the V-band is in agreement with the results published in the literature, even with the radiometric-derived albedo. This stellar occultation has allowed for the first multichord measurement of a large topography in a TNO.

Key words. Kuiper belt: individual: 2002 MS₄ – Methods: observational

1. Introduction

Trans-Neptunian objects (TNOs) are small Solar System bodies that orbit the Sun with a semi-major axis larger than that of Neptune (Jewitt et al. 2008). Due to the low spatial density of material in this orbital region and the significant distance from the Sun, their global physical-chemical composition has been largely unaffected since their formation. Therefore, they are considered to be remnants of the primordial disk and a valuable source of information about the primitive solar nebula and the evolution of our planetary system (Gladman et al. 2008; Morbidelli et al. 2008; Nesvorný & Morbidelli 2012). In addition, knowledge of the size-frequency distribution of TNOs allows for constraints to be placed on Solar System formation models (Petit et al. 2008). Mainly due to the faintness and small angular sizes seen from Earth, our knowledge of the fundamental physical properties of the TNO population is still scarce and fragmented (Stansberry et al. 2008; Lellouch et al. 2013; Lacerda et al. 2014). Since the discovery of (15760) Albion in 1992 (Jewitt & Luu, 1993), thousands of objects have been observed in this orbital region. However, the size and albedo of only 178 Centaurs (objects with unstable orbits between Jupiter and Neptune) and TNOs have been determined using thermal observations (Müller, Lellouch, and Fornasier 2020). On the other hand, spacecraft visits can fully characterize these objects, as in the case of the visit of the New Horizons mission (Weaver and Stern 2008) to the Pluto system (Stern et al. 2015, 2020; Spencer et al. 2020 b) and (486958) Arrokoth (Stern et al. 2019; Benecchi et al. 2019; Buie et al. 2020 a; Spencer et al. 2020 a), which allowed for detailed studies. However, the aforementioned approaches require significant investment and cannot be used to study a larger number of objects.

Stellar occultation is an efficient ground-based method to study dozens of these distant bodies. It consists of observing a background star while a small body passes in front of it and blocks the stellar flux for several seconds. An updated list of Lucky Star stellar occultation detections (that we are aware of) can be found in the SOSB Database¹ (Braga-Ribas et al. 2019). These observations provide an instantaneous limb of the object that can be combined with information derived from other observational methods to better characterize the small body (Ortiz et al. 2020b).

In this work, we predicted, observed, and analyzed nine stellar occultations by the large TNO (307261) 2002 MS₄ (hereafter denoted as MS4 for brevity). It was discovered by the Near-Earth Asteroid Tracking (NEAT)² program on June 18, 2002, and is classified as a hot classical TNO due to its high orbital inclination (Gladman et al. 2008; Van Laerhoven et al. 2019). Furthermore, MS4 is a candidate to be a dwarf planet due to its thermally derived equivalent diameter (Vilenius et al. 2012). Physical and orbital parameters taken from previously published works are listed in Table 1.

Table 1: Orbital and physical properties of MS4 from the literature.

Orbital properties ^a		Physical properties	
a	41.8 au	D ^b	934 ± 47 km
q	35.75 au	H _V	4.0 ± 0.6 ^b / 3.63 ^c
i	17.7°	p _V ^b	0.051 ^{+0.036} _{-0.022}
e	0.14	A _p mag ^d	20.39 mag

Notes. ^(a) Orbital elements from JPL Small-Body Database Browser web page (https://ssd.jpl.nasa.gov/tools/sbdb_lookup.html/#?sstr=2002MS4). ^(b) Physical properties obtained by Vilenius et al. (2012): area-equivalent diameter (**D**) and geometric albedo at V-band (**p_V**); **H_V**: average absolute magnitude at V-band; Stansberry et al. (2008) obtained D = 726.05 ± 123.05 km and p_V = 0.084^{+0.038}_{-0.023} for a value of H_V = 4.0 using Spitzer data only. ^(c) Information from Tegler et al. (2016). ^(d) **A_pmag**: object's average apparent visual magnitude on August 8, 2020, from JPL website <https://ssd.jpl.nasa.gov/horizons/app.html/#/>.

2. Predictions and observations

We performed classical astrometric runs to refine MS4's ephemeris at the Pico dos Dias (Brazil), La Silla (Chile), Calar Alto (Spain), and Pic du Midi (France) observatories between 2009 and 2019. The updated ephemeris and the *Gaia* Data Release 1 catalog (Gaia Collaboration et al. 2016 a,b, 2018) significantly improved the prediction of the July 9, 2019 occultation, resulting in our first occultation by MS4. Furthermore, the astrometry derived from this occultation data improved the subsequent predictions.

In 2019, we observed four stellar occultations by MS4 from Argentina, Brazil, Canada, and Chile (see Tables B.4 and B.5). On July 26, we obtained a multichord detection from three well-separated sites and about eight hours later, a single-chord occultation of a different star from Canada. On July 9 and August 19, we detected two positive chords and a set of negatives. The astrometric results from 2019 data (Table 5) were used to calculate new ephemeris and predict the subsequent events using the Numerical Integration of the Motion of an Asteroid (NIMA) tool described on Desmars et al. (2015)³

The first observation in 2020 was a double chord from South Africa on July 26, which confirmed the accuracy of MS4's ephemeris at an eight-milliarcsec (mas) level. Therefore, we organized an extensive campaign and successfully observed, from 61 sites, an occultation of a bright star (V = 14.62 mag) on August 8, 2020. As described in this work, we derived valuable physical information from this multichord event observed in North Africa, Europe, and Western Asia. After the 8 August 2020 campaign, three other events were observed on 24 February 2021, 14 October 2021, and 10 June 2022. Single, double, and triple detections, respectively (Tables B.4 and B.5). Those data and equipment information collection processes were carried out through the Occultation Portal⁴ (Kilic et al. 2022). Table 2 shows the relevant information about all the occulted stars from the *Gaia* Data Release 3 catalog (GDR3, Gaia Collaboration et al. 2023).

The default procedure for all events was to update the prediction and send alerts to potential observers within or close to the predicted shadow path. However, an exception was made for

* Tables B.1, B.2, B.3, B.4, and B.5 are only available in electronic form at the CDS via anonymous ftp to cdsarc.cds.unistra.fr (130.79.128.5) or via xxxxxx

** Fulbright Visiting Scholar (2022 - 2023) at University of California, Berkeley

¹ Stellar Occultation by Small Bodies database is available on <http://occultations.ct.utfrp.edu.br/results>

² More information available at <https://sbn.psi.edu/pds/resource/neat.html>

³ MS4's ephemeris (NIMA v9) is publicly available on <https://lesia.obspm.fr/lucky-star/obj.php?p=692>.

⁴ More information on <https://occultation.tug.tubitak.gov.tr/about/>

the 8 August 2020 occultation due to favorable circumstances. A campaign web page with helpful information for the observers was built⁵. Also, alerts were sent to all individuals with access to portable or professional telescopes and near or inside the predicted shadow path, resulting in such a large number of positive detections.

The data came from a wide range of telescopes, from small portable ones (apertures between 13 cm and 30 cm) to large facilities such as the 4.1 m telescope at the Southern Astrophysical Research (SOAR, Chile), the 2 m Liverpool telescope at Roque de Los Muchachos (Spain), the 1.6 m telescope at Pico dos Dias (Brazil), and the 1.5 m telescope at Sierra Nevada (Spain) observatories. Most observers did not use filters to maximize photon fluxes on the CCD and so, they were able to a better signal-to-noise ratio (S/N). Even though some observers used the Global Positioning System (GPS) to acquire the time, the most common time source was the computer clock synchronization with a Network Time Protocol (NTP). A compilation of all the participating observers and instruments is presented in Appendix B. All the predictions and observational efforts were developed in the framework of the European Research Council (ERC) *Lucky Star* project⁶.

3. Data reduction, analysis, and results

The great diversity of telescopes and detectors was reflected in five data formats⁷: *avi*, *adv* (Pavlov et al. 2020), *ser*, *cpa*, and FITS. Most *avi*, *adv*, and *ser* video files were converted to FITS images using TANGRA⁸ software. However, from some videos, the images were extracted using a proprietary PYTHON 3 script based on ASTROPY v4.0.1 (Astropy Collaboration et al. 2013). When calibration images were available, the raw images were corrected from any bias, dark, and flat-field using standard procedures with the Image Reduction and Analysis Facility (IRAF, Butcher & Stevens, 1981).

We applied aperture photometry on the target and some comparison stars on all the FITS files using the Package for the Reduction of Astronomical Images Automatically (PRAIA, Assafin et al. 2011, 2023). The chosen photometric apertures considered the maximization of the S/N. The light curve obtained for the target star, which includes less than 1% of flux contributions from MS4, is then divided by the averaged light curves of the comparison stars to account for sky transparency variations in the data. Also, the flux outside the occultation is normalized to unity by fitting a polynomial function. Finally, the ingress and egress times were derived using the standard chi-square method (χ^2 test) between the observed and a synthetic light curve implemented in the Stellar Occultation Reduction and Analysis package, v0.2.1 (SORA, Gomes-Júnior et al. 2022). The synthetic light curve considers a sharp-edge model convolved with Fresnel diffraction, finite exposure time, CCD bandwidth, and stel-

lar diameter at MS4's distance (details about this procedure are available in Gomes-Júnior et al. 2022 and references therein). The stellar diameters projected at MS4 distance were calculated according to Kervella et al. (2004)'s formalism and are listed in Table 2. Organized by the occultation date, Table 3 contains the ingress and egress times (UTC) with 1σ uncertainties for each station with a positive detection. Appendix C presents the normalized and the synthetic light curves used to obtain the occultation timings.

If not differentiated, large TNOs such as MS4 may reach one of the hydrostatic equilibrium shapes: the Jacobi three-axial ellipsoid or the Maclaurin oblate spheroid (Chandrasekhar 1987; Tancredi and Favre 2008). The apparent global limb of the body is then an ellipse projected in the sky plane, defined by $M = 5$ free parameters: center offset relative to the ephemeris (f and g), the semi-major axis (a'), the semi-minor axis (b'), or equivalently, the oblateness [$\epsilon' = (a' - b')/a'$], and the position angle (PA) of b' . The PA counts positively, starting from the celestial north and increasing to the east. We converted the ingress and egress times into a stellar position for each stellar occultation event, with f and g increasing toward celestial east and north, respectively. At this point, we can fit a limb model to these points, which provides, among others, the position of MS4's center in the sky plane and, thus, an ephemeris offset.

Among the nine stellar occultation events, only three allow for an elliptical fit to the chords, namely: 9 July 2019, 8 August 2020, and 10 June 2022. We started our fitting procedure with the 61 chords acquired on 8 August 2020 (Sect. 3.1), and we then used the residuals of the elliptical limb fit to search for topographic features on MS4 (Sect. 3.2). Finally, we compared the resulting global ellipse with the chords observed in the other events (Sect. 3.3).

3.1. 8 August 2020

Three circumstances triggered an extensive observational campaign for this occultation: i) the bright target star ($G = 14.6$ mag from GDR3 catalog), ii) a milliarcsecond-level accuracy of MS4's ephemeris stemming from previously detected occultations, and iii) a shadow path crossing densely populated regions. Accordingly, the observational campaign motivated the participation of 116 telescopes from Europe, North Africa, and Western Asia. As a result, we received 61 positive and 40 negative data sets. The other 15 locations had bad weather conditions, and observers could not acquire data. The number of effective chords is smaller than the 61 positives due to overlapping observations from nearby observatories along the object's limb.

We then submitted all the images to the procedure described at the beginning of this section. As absolute time acquisition is essential to achieve good results, we checked each data set and applied offsets when: i) the observer reported time issues during the acquisition, ii) the camera acquisition software is known to have a systematic offset, and iii) overlapped chords that do not match the ingress and egress instants. In this last case, the time shifts applied to the original positive data were based on comparison with close-by chords. All the time shifts are presented in Table B.1, and the corrected instants are in Table 3. Figure 1 shows all the positives (blue lines) and their uncertainties in ingress and egress times (red segments).

A simple elliptical model cannot effectively reproduce the observed profile projected at the sky plane. However, a global profile can be obtained by selecting 13 positive chords among the 61 positives. The first selection criterion was the time source, namely, data acquired with GPS were preferred. Among the 17

⁵ The campaign web page is available in https://lesia.obspm.fr/lucky-star/campaigns/2020-08-08_2002MS4.html

⁶ <https://lesia.obspm.fr/lucky-star/>

⁷ *avi* = Audio Video Interleave. Information for the *adv* (Astronomical Digital Video) can be found in https://www.iota-es.de/JOA/JOA2020_3.pdf. The documentation for the simple image sequence format known as *ser* can be found in <http://www.grischa-hahn.homepage.t-online.de/astro/ser/>. *cpa* is a compressed image file associated with PRISM (<http://www.prism-astro.com/fr/index.html>). The most recent Flexible Image Transport System-FITS documentation can be found in https://fits.gsfc.nasa.gov/fits_standard.html

⁸ <http://www.hristopavlov.net/Tangra3/>

Table 2: Target stars designation and geocentric coordinates at closest approach instant (UT) sorted by occultation date (day-month-year).

Date	Gaia DR3 Designation	Propagated right ascension (hh mm ss.sssss)	Error (mas)	Propagated declination (° ' ")	Error (mas)	V ^a (mag)	K ^a (mag)	S _{Diam} ^b (km)	Δ _{MS4} ^c (au)
09-07-2019	4253196402592965504	18 45 19.24565	0.15	-06 24 13.0031	0.12	15.00	14.15	0.19	45.62
26-07-2019	4253186506987951104	18 44 07.57274	0.54	-06 26 40.1240	0.46	17.78	16.27	0.08	45.67
	4253186477047835648	18 44 06.31756	0.13	-06 26 43.8948	0.11	15.45	11.66	0.98	45.68
19-08-2019	4253181804071259648	18 42 43.51905	0.24	-06 32 34.0868	0.19	16.51	16.59	0.05	45.88
26-07-2020	4253244201379441792	18 48 18.07372	0.12	-06 13 31.6134	0.12	14.76	12.61	0.47	45.60
08-08-2020	4253248324549054464	18 47 29.96384	0.12	-06 16 31.4727	0.10	14.62	11.13	1.19	45.70
24-02-2021	4253709191700784896	18 56 35.98731	0.25	-06 30 23.1569	0.23	16.51	12.96	0.53	47.05
14-10-2021	4252495635735083264	18 50 30.76176	0.31	-06 24 13.3375	0.27	15.83	13.44	0.34	46.52
10-06-2022	4253907305577009664	19 00 15.44628	0.23	-05 42 42.9960	0.21	15.1	13.00	0.39	45.48

Notes. It is essential to mention that none of the stars have a duplicity flag in the *Gaia* DR3 catalog. ^(a) The magnitudes retrieved from NOMAD catalog and used in SORA to calculate the ^(b) stellar diameter (S_{Diam}) at the ^(c) MS4's geocentric distance (Δ_{MS4}).

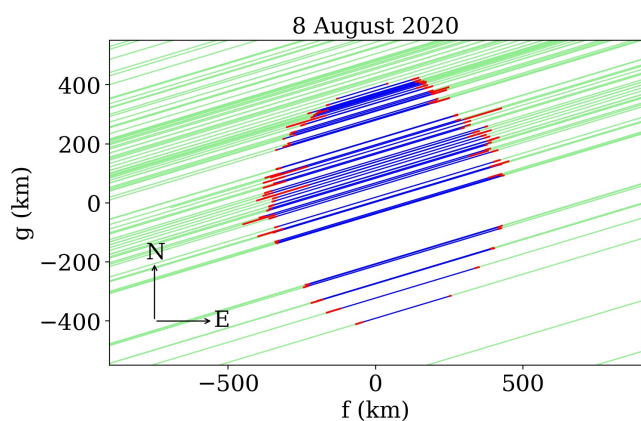


Fig. 1: Chords measured during the 8 August 2020 event show the detection of MS4's limb in blue with 1σ error bars (red segments). Six positive chords with large error bars were suppressed from this plot for better visualization: TAROT, Lleida, Khmelnytskyi, Fuensanta de Martos, Kharkiv T36, and Marbella. The green lines represent positions compatible with the total target's flux within the noise (i.e., no secondary occultation). The order of positive chords, from north to south, is the same as in Table 3.

GPS data sets, we discarded the following: 1) Varages because it presented a gradual emersion in the light curve (see Sect. 3.2); 2) Nice due to reported time issues during the acquisition; 3) Khmelnytskyi and Sevilla because it probed the latitude where a large topography is suspected (see Sect. 3.2); 4) Guaricino because the GPS was connected to the computer and it presented a large offset with respect to all close-by chords; 5) Artemis because its length does not match the length of Catania's chord (at 1σ level), which probed exactly the same object's profile but is a bit larger. 6) Finally, Caussols, Ariana, and Kuban have larger uncertainties than other chords that probed the same region. In addition to the eight GPS data sets, we selected another five positive chords acquired from Méo station, Mátraszentistván, Hvar, Agerola, and La Palma. The main criteria for selecting the mentioned NTP chords were: data acquired with professional telescopes, low dispersion in the light curves, and the smallest uncertainties of the probed limb.

Figure 2 presents the 13 selected positive chords (blue) overplotted to the other positives (gray segments). Solid lines represent GPS chords, while dashed lines show NTP data. The se-

lected data are ordered from north to south, as follows: Méo station (FRA), Valbonne (FRA), Mátraszentistván (HUN), Catalonia (ESP), Massa (ITA), Rome (ITA), Hvar (HRV), Sassari (ITA), Odesa (UKR), Agerola (ITA), Algiers (DZA), La Palma (ESP), and Çanakkale (TUR). They provide $N = 26$ independent points at the sky plane to fit the five ellipse parameters. The global elliptical limb is determined by minimizing the classical χ^2 function. The quality of the result is given by the χ^2 per degree of freedom $\chi^2_{\text{pdf}} = \chi^2 / (N - M) \approx 1$ for satisfactory fits, where N is the number of points and M is the number of fitted parameters (Gomes-Júnior et al. 2022). A set of empirical tests⁹ assuming topography values between 0 and 10 km were performed and revealed a good fit ($\chi^2_{\text{pdf}} = 0.92$) when features of 7 km were considered. This result agrees with the theoretical approach proposed by Johnson and McGetchin (1973), which gives a lower limit of 6 to 7 km for topography on MS4 (see Sect. 3.4).

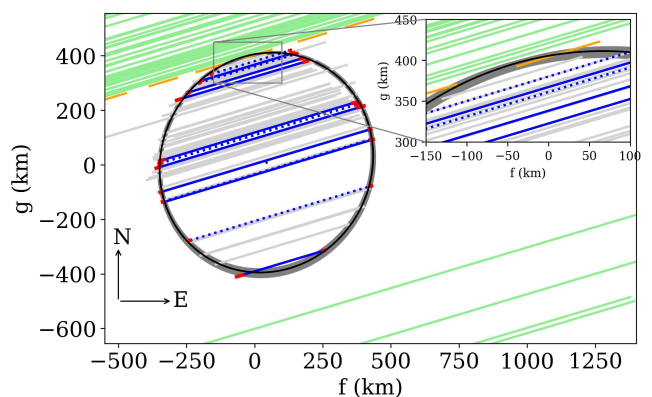


Fig. 2: Thirteen selected chords (blue), where GPS data are presented in solid lines and NTP by dashed lines. Gray segments show the other positive chords not used in limb-fitting. The black ellipse shows the best elliptical limb, and the gray region the solutions within 3σ . The orange segments represent each image acquired from the Montsec station and the light green segments show other negative chords.

Among the elliptical solutions inside the 3σ region, we excluded those that crossed or approached the negative grazing

⁹ See Eq. 11 in Gomes-Júnior et al. (2022) for details about the function that considers topography in the limb fitting.

Table 3: Ingress and egress instants with 1σ error bars.

Sites	Ingress (hh:mm:ss.ss \pm ss.ss)	Egress (hh:mm:ss.ss \pm ss.ss)
09 July 2019		
OPSPA	04:23:28.65 \pm 0.19	04:23:58.26 \pm 0.38
ASH2	04:23:27.2 \pm 1.1	04:23:56.73 \pm 2.1
Pico dos Dias	04:22:02.182 \pm 0.006	04:22:29.44 \pm 0.67
26 July 2019 - South America		
OPSPA	02:47:15.6 \pm 7.8	02:48:04.0 \pm 3.7
ASH2	02:47:21.0 \pm 3.8	02:47:54.8 \pm 5.3
Paranal	02:47:34.33 \pm 0.12	02:48:07.9 \pm 1.2
Pico dos Dias	02:45:55.310 \pm 0.099	02:46:17.581 \pm 0.093
26 July 2019 - North America		
Osoyoos	10:15:16.65 \pm 0.40	10:15:53.12 \pm 0.33
19 August 2019		
Penticton	07:37:19.2 \pm 2.6	07:37:55.2 \pm 1.3
Osoyoos	07:37:17.55 \pm 0.55	07:37:53.7 \pm 2.0
26 July 2020		
Pretoria	23:15:28.46 \pm 0.12	23:15:54.27 \pm 0.15
Johannesburg	23:15:28.940 \pm 0.092	23:15:55.89 \pm 0.18
08 August 2020		
Varages	20:43:44.858 \pm 0.058	20:43:53.359 \pm 0.028
TAROT North	20:43:39.5 \pm 2.0	20:43:51.5 \pm 2.0
Méo station	20:43:39.488 \pm 0.021	20:43:53.960 \pm 0.027
Caussols	20:43:39.27 \pm 0.13	20:43:54.18 \pm 0.56
Lleida	20:44:01.4 \pm 6.6	20:44:25.13 \pm 0.12
Cannes	20:43:37.23 \pm 0.21	20:43:55.64 \pm 0.39
Nice	20:43:36.444 \pm 0.029	20:43:52.834 \pm 0.071
Valbonne	20:43:37.376 \pm 0.055	20:43:54.07 \pm 0.13
Črni Vrh	20:43:09.71 \pm 0.94	20:43:26.58 \pm 0.35
Mátraszentistván	20:42:46.866 \pm 0.015	20:43:04.739 \pm 0.045
Ljubljana	20:43:06.70 \pm 0.20	20:43:25.20 \pm 0.33
Budapest	20:42:49.59 \pm 0.13	20:43:08.61 \pm 0.20
Trieste	20:43:07.7 \pm 3.3	20:43:27.41 \pm 0.85
Catalonia	20:43:57.15 \pm 0.21	20:44:17.84 \pm 0.14
Bologna	20:43:17.40 \pm 0.26	20:43:38.77 \pm 0.67
Massa 02	20:43:20.52 \pm 0.39	20:43:43.83 \pm 0.32
Castelvecchio Pascoli	20:43:18.742 \pm 0.088	20:43:44.1 \pm 1.4
Borgo a Mozzano	20:43:19.224 \pm 0.078	20:43:42.80 \pm 0.12
San Marcello Pistoiese	20:43:16.200 \pm 0.072	20:43:42.6 \pm 1.2
Sta. Maria a Monte	20:43:17.68 \pm 0.12	20:43:42.80 \pm 0.11
Signa	20:43:15.61 \pm 0.57	20:43:40.38 \pm 0.67
Lastra a Signa	20:43:13.815 \pm 0.084	20:43:41.9 \pm 1.2
Khmelnyskiy	20:42:01.81 \pm 0.82	20:42:49.7 \pm 15.7
Sevilla	20:44:29.03 \pm 0.13	20:44:59.40 \pm 0.19
Huelva	20:44:32.74 \pm 0.37	20:45:02.72 \pm 0.28
Cluj-Napoca	20:42:25.0 \pm 1.2	20:42:56.61 \pm 0.30
Fuensanta de Martos	20:44:22.0 \pm 3.0	20:44:55.0 \pm 3.1
Fiastra	20:43:05.1 \pm 1.8	20:43:37.89 \pm 0.52
Dragsina	20:42:32.938 \pm 0.087	20:43:05.82 \pm 0.32
Ibiza	20:43:56.6 \pm 1.8	20:44:28.55 \pm 0.24
Alhendín	20:44:17.89 \pm 0.57	20:44:54.83 \pm 0.18
Granada (150 cm)	20:44:17.571 \pm 0.008	20:44:52.08 \pm 0.51
Granada (90 cm)	20:44:16.53 \pm 0.51	20:44:51.755 \pm 0.026
Estepona	20:44:24.37 \pm 0.45	20:45:00.4 \pm 1.9
Marbella	20:44:26.1 \pm 4.3	20:44:59.64 \pm 0.22
Rome	20:43:08.37 \pm 0.37	20:43:43.79 \pm 0.37
Hvar	20:42:51.69 \pm 0.21	20:43:27.96 \pm 0.35
Bacau	20:42:12.60 \pm 0.30	20:42:50.49 \pm 0.72
Sassari	20:43:19.35 \pm 0.35	20:43:56.60 \pm 0.50
Guarcino	20:43:03.86 \pm 0.15	20:43:41.13 \pm 0.15
Kharkiv (70 cm)	20:41:40.00 \pm 0.13	20:42:17.16 \pm 0.12
Kharkiv (36 cm)	20:41:39.6 \pm 1.9	20:42:18.3 \pm 1.2
Ceccano	20:43:02.39 \pm 0.41	20:43:40.76 \pm 0.37
Brasov	20:42:14.2 \pm 2.7	20:42:51.5 \pm 1.6
Bárlad	20:42:09.23 \pm 0.55	20:42:47.00 \pm 0.49
Valenii de Munte	20:42:15.14 \pm 0.24	20:42:52.61 \pm 0.50
Ploiesti	20:42:14.25 \pm 2.1	20:42:53.2 \pm 1.5
Odesa	20:42:00.00 \pm 0.14	20:42:38.49 \pm 0.11
Sorrento	20:43:00.66 \pm 0.30	20:43:37.7 \pm 1.1
Agerola	20:42:59.603 \pm 0.050	20:43:37.842 \pm 0.093
Algiers	20:43:50.844 \pm 0.021	20:44:29.115 \pm 0.075
La Palma	20:45:35.032 \pm 0.014	20:46:08.313 \pm 0.018
Tijarafe	20:45:35.68 \pm 0.19	20:46:08.08 \pm 0.11
Ariana	20:43:23.87 \pm 0.29	20:43:56.80 \pm 0.25
Artemis	20:45:31.938 \pm 0.022	20:46:01.297 \pm 0.024
TAR 1	20:45:32.360 \pm 0.057	20:46:01.595 \pm 0.063
Catania	20:43:04.59 \pm 0.92	20:43:34.564 \pm 0.085
Kuban	20:41:36.2 \pm 1.2	20:42:00.63 \pm 0.31
Çanakkale	20:42:23.39 \pm 0.56	20:42:38.830 \pm 0.072
24 February 2021		
OPSPA	08:41:37.00 \pm 0.61	08:42:09.182 \pm 0.082
ASH2	08:41:36.82 \pm 0.98	08:42:08.43 \pm 0.30
14 October 2021		
Osoyoos	03:23:30.14 \pm 0.40	03:24:35.33 \pm 0.67
Flagstaff	03:25:54.61 \pm 0.44	03:26:39.33 \pm 0.73
10 June 2022		
La Palma	05:30:08.475 \pm 0.091	05:30:43.30 \pm 0.13
Artemis	05:30:02.427 \pm 0.066	05:30:37.51 \pm 0.49
Tree Gate Farm	05:34:47.18 \pm 0.33	05:35:22.12 \pm 0.28

Notes. The times are sorted from northernmost to southernmost observatories regarding the object's probed latitude and divided by date.

chords within the tolerance level of 7 km (radial direction). Therefore, although the solutions cross the negative chord as seen from Montsec (Fig. 2), they are inside the 7 km assumed range. The area equivalent radius was calculated using the relation $R_{\text{equiv}} = a' \sqrt{1 - \epsilon'}$. Finally, the limb solution in Table 4 represents the best-fitted elliptical limb at the sky plane with uncertainties at the 3σ level.

Table 4: Parameters of the best-fitted ellipse (at 3σ level) derived from the 13 selected positive chords from the August 8 event.

MS4's global elliptical limb ^a					
f	43 \pm 6 km	a'	412 \pm 10 km	PA	121 \pm 16°
g	7 \pm 9 km	ϵ'	0.066 \pm 0.034	R_{equiv}	398 \pm 12 km

Notes. ^(a) These solutions admit topographic features up to 7 km and are limited to the north by the negative chord from the Montsec station (orange segments in Fig. 2).

A general view of the August 2020 event is shown in Fig. 3. The blue lines represent the observed shadow path. It is worth mentioning that the 13 selected chords are in blue circles, and the other positives are in red triangles. We note that a black star marks the negative detection by Montsec station, while the green triangles mark the other negatives observations.

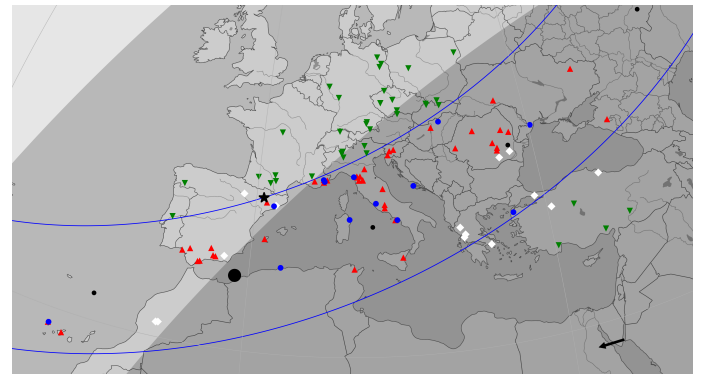


Fig. 3: Post-occultation map showing the location of each station that participated in the 8 August 2020 occultation campaign. Solid lines delimit the observed shadow path, and the black dots mark the shadow position every minute, with the largest at the moment of the geocenter's closest approach. The shadow follows the direction given by the black arrow. The blue dots indicate the 13 selected chords, while the other positives are in red triangles. A black star marks the close-by negative chord acquired from Montsec station. Green triangles and white diamonds represent stations with negative data and bad weather, respectively.

3.2. Topographic features

Determining the topographic limits for small bodies in the outer Solar System is challenging. The first attempts were theoretical; for instance, Johnson and McGetchin (1973) proposed a method to determine topography limits for planetary satellites using their global density and composition. On the other hand, from an observational point of view, just a few small bodies orbiting the Sun beyond Neptune had their topography limits set using stellar occultations (Dias-Oliveira et al. 2017; Leiva et al. 2017). Also, with the advance in interplanetary spacecraft technology, the surface of a few objects was studied using in situ images.

For instance, using Voyager’s images of Uranus’s largest satellites Schenk and Moore (2020) found superficial features up to 11 km. Likewise, New Horizons’ flyby over the Pluto system (Moore et al. 2016; Nimmo et al. 2017) and (486958) Arrokoth (Spencer et al. 2020 a) revealed superficial structures on the same scale.

Applying the theoretical approach mentioned above for MS₄ and assuming an icy body with a density between $\rho = 1.0 - 2.0 \text{ g.cm}^{-3}$, the lower limit for superficial features is 6 to 7 km. If material strength may increase toward the nucleus, the surface might support more prominent features. Also, considering the sizes of the structures observed by spacecraft in other objects, assuming features up to 7 km on MS₄’s surface is reasonable.

The first evidence of topography was observed in the Varages light curve. This data set does not have dead time between the images, and each exposure translates into a resolution of 1.97 km into the sky plane. The Fresnel diffraction and stellar diameter at MS₄ geocentric distance are at the same level, 1.54 km and 1.19 km, respectively. The mentioned light curve presents a sharp ingress and a gradual egress above the noise level, as shown in Fig. 4. The feature did not appear in the other high S/N light curves, thus weakening the possibility of a secondary star. Therefore, the most plausible explanation is a topography where a portion of the star appeared a few frames before egress, corresponding to ≈ 10 km-long feature in the chord’s direction. The insert in Fig. 4 displays the stellar position in each frame, represented by yellow circles, relative to a proposed limb in gray.

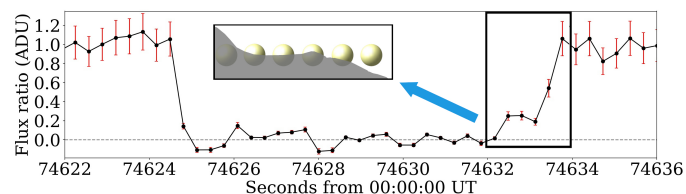


Fig. 4: Normalized stellar flux in each frame acquired in Varages station as a function of time in black dots, with photometric uncertainties in red. The insert selects the egress region and illustrates a possible explanation for such a signal (see text).

The second evidence of topography on MS₄’s observed limb comes when investigating the residuals of the average ellipse presented before. Some groups of points between $\text{PA} = -5^\circ$ and $\text{PA} = 120^\circ$ presented a large offset regarding the global limb. Therefore, to better describe this local limb, we built a model based on a combination of symmetric parabolas, the simplest function that can reproduce the observed features. Equations 1 and 2 provide the models used to fit the group of points with negative and positive dispersion (R_D), respectively. The y term defines the parabola’s depth and height, when positive indicates depression. The x term is related to the parabola’s curvature. PA is the position angle, and z accounts for the parabola’s distance from the plot’s origin. The model’s R_D values outside the topography region are defined as being zero.

$$\text{Depression} = \begin{cases} 0 & R_D \geq 0, \\ x(\text{PA} - z)^2 - y & R_D < 0. \end{cases} \quad (1)$$

$$\text{Elevation} = \begin{cases} 0 & R_D \leq 0, \\ x(\text{PA} - z)^2 + y & R_D > 0. \end{cases} \quad (2)$$

Then, the model is built by summing the equations,

$$\text{Model} = \text{Depression} + \text{Elevation} + \text{Depression},$$

where one depression corresponds to the Varages egress region (shown here as negative position angles for better viewing).

The fitting was made using a high-level PYTHON interface named LMFIT¹⁰, designed for non-linear optimization and curve-fitting problems. First, we used the differential evolution (DE) minimization method (Storn and Price 1997) to derive the first estimation of the model’s parameters, which can explore large areas of candidate space without getting stuck in a local minimum. Then, to get a representative estimation of the model’s uncertainties, we explored the parameter space using the maximum likelihood via Monte Carlo Markov chain sampler: *emcee*¹¹ (Foreman-Mackey et al. 2013). The center of each feature was limited as follows: main depression between $40^\circ \pm 20^\circ$, elevation between $7.5^\circ \pm 7.5^\circ$, while the Varages depression was fixed on $\text{PA} = -3.9^\circ$. The model section between -5° and 0° does not have significant errors due to the precision of the grazing detection presented in Fig. 4. For this angle interval, we do not allow the sampler to estimate for unknown uncertainties. However, for the elevation and the main depression, *emcee* found that unknown uncertainties must be about 4.5 km. This value is reasonable, considering that the 7 km of tolerance assumed during the global fit was not included in the points error bars.

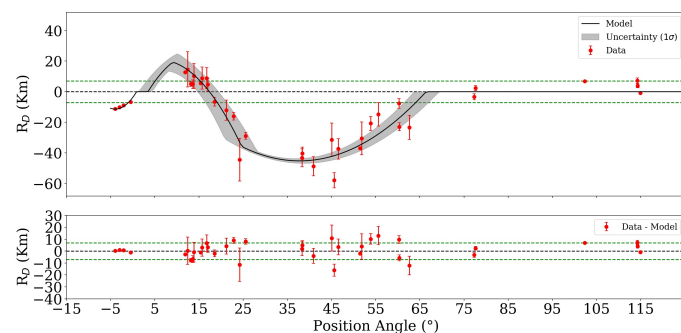


Fig. 5: Limits of the assumed ± 7 km tolerance (see text) shown as horizontal green lines and the black dashed line is the best-fit ellipse. **Upper panel:** Red points (R_D) are the distance of each point from the best-fit ellipse (in the normal-to-the-ellipse direction) as a function of the position angle, and the solid black line is the model with 1σ uncertainty represented in gray. **Lower panel:** Residuals after subtracting the model from the data points.

After subtracting the model from the data set, residuals are inside the expected range (bottom panel in Fig. 5). Therefore, according to the model at 1σ level, MS₄’s surface has an ≈ 11 km depth depression in the region detected by Varages station, followed by an elevation of 25_{-5}^{+4} km. However, the most impressive feature is the 45.1 ± 1.5 km depth depression with a linear extension of 322 ± 39 km. Figure 6 presents a general view of the detected limb and summarizes the topography solutions. However, because the depression was likely not in its middle position at the limb, it is likely more extensive and profound than what it seems from this snapshot at a particular rotation phase. Such prominent superficial features may be caused by collisions with other small objects.

¹⁰ More about this library can be found in the <https://lmfit.github.io/lmfit-py/>

¹¹ Documentation available on <https://emcee.readthedocs.io/en/stable/>

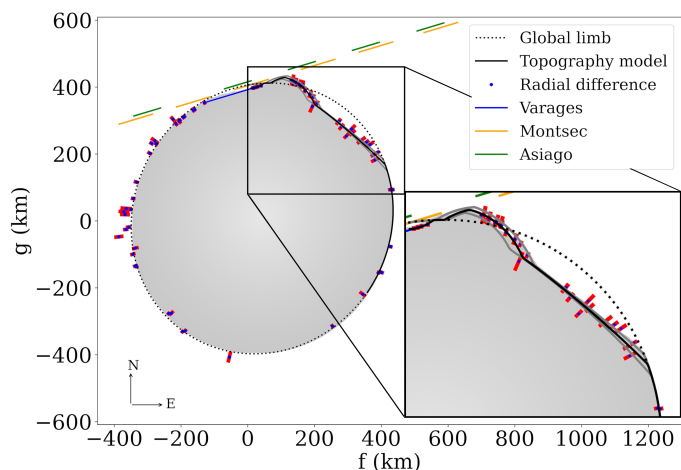


Fig. 6: R_D points projected at the sky plane in blue points, with 1σ uncertainties in red. The blue segment is the positive detection from Varages station. Orange and green segments correspond to negative frames acquired in Montsec and Asiago stations, respectively. In black, the dotted line is the best-fitted global limb model described in Sect. 3.1, and the solid line is the model for local topography. The solid gray lines limit the topographic model's 1σ -error bars. Finally, the filled gray color shows the proposed global limb with topography.

3.3. Other occultation events

An object's 3D shape is strongly correlated with the body's rotational modulation (Chandrasekhar 1987; Tancredi and Favre 2008). For example, Maclaurin objects usually have single-peaked rotational light curves with small peak-to-peak amplitudes caused by albedo features. In contrast, the rotational light curve of a Jacobi shape presents double-peaked curves with more pronounced amplitudes (unless they are seen nearly pole-on). Therefore, a reasonable determination of MS4's rotational parameters is crucial to derive an accurate 3D size, shape, albedo, and density.

However, MS4 has crossed a highly dense field of stars since its discovery. Therefore, it is complicated to obtain precise photometric measurements because it is usually blended with faint background stars (as seen from Earth). However, in 2011 it passed in front of a dark cloud when it was observed well isolated from other stars in about 100 images. Using those images along with a data set acquired in the Sierra Nevada observatory, Thirouin (2013) derived a single-peaked light curve with an amplitude of 0.05 ± 0.01 mag and two possibilities for the rotational period: 7.33 h or 10.44 h. Such a small amplitude may indicate that MS4 is a Maclaurin object. It is also possible that it is a triaxial body, such as a Jacobi ellipsoid observed close to a pole-on orientation. Considering the observed small amplitude and small change in the aspect angle, the projected area on the sky plane between 2019 and 2022 should not change considerably. Nevertheless, if it is a triaxial object, the position angle of the projected ellipse on each observed occultation will present significant changes according to its rotational phase.

Due to its large diameter and small rotational light curve amplitude, the Maclaurin spheroid is our preferred 3D shape for MS4. Thus, we tried fitting the same 3σ solution derived from the 8 August 2020 event (Table 4) on the chords obtained on the other occultation events. Using χ^2 minimization, the ellipse was fitted with the center (f and g) as a free parameter. When

two center positions are equally possible (single chord cases), we present the center solution closer to the position predicted by the NIMA v9 ephemeris. Figures 7 and 8 show the results of the limb fitting for the other eight events. Table 5 presents the derived astrometric information, and Appendix A shows the post-occultation maps with the observed shadow path and station locations.

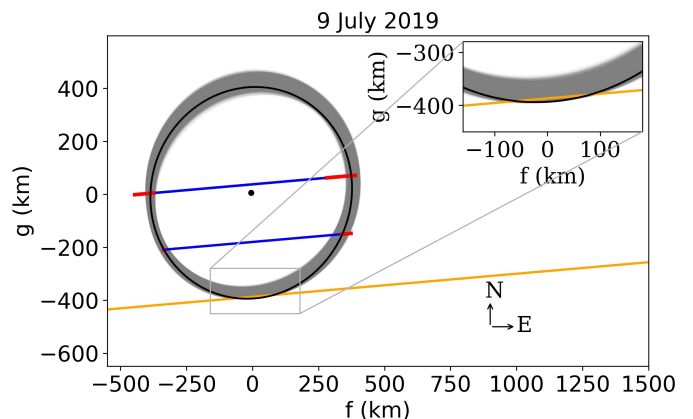


Fig. 7: Positive data from the stellar occultation on 9 July 2019 shown as the blue segments. The 1σ uncertainties are in red, and the negative chord acquired from the Ponta Grossa station is in orange. The best-fitted ellipse is in black, with the center presented by the black dot, and the solutions in the 3σ range are in gray. The fit considers topographic features up to 7 km in size. Thus, the ellipses crossing the negative chord are in this range.

Table 5: Astrometric information (ICRS) for the geocentric closest approach instant (UT) obtained from the nine stellar occultation events observed between 2019 and 2022, sorted by date (day-month-year).

Date	Instant (UT) (hh:mm:ss.ss)	Right ascension (hh mm ss.ss)	Error (mas)	Declination (° ' ")	Error (mas)
09-07-2019	04:23:49.08	18 45 19.245981	0.23	-06 24 13.05928	0.60
26-07-2019	02:47:08.52	18 44 07.573463	0.57	-06 26 40.17686	0.51
26-07-2019	10:18:43.02	18 44 06.315990	0.37	-06 26 43.7686	1.3
19-08-2019	07:41:52.28	18 42 43.51613	1.0	-06 32 33.9776	1.1
26-07-2020	23:17:56.04	18 48 18.075014	0.12	-06 13 31.70897	0.12
08-08-2020	20:44:27.26	18 47 29.961308	0.12	-06 16 31.34442	0.10
24-02-2021	08:45:52.82	18 56 35.9873	1.1	-06 30 23.1583	2.8
14-10-2021	03:26:05.50	18 50 30.768595	0.48	-06 24 13.20676	0.52
10-06-2022	05:32:47.30	19 00 15.446841	0.32	-05 42 42.8843	1.3

3.4. MS4's size, shape, and albedo

As mentioned previously in this work, we consider MS4 to have a Maclaurin shape ($a = b > c$) with an equatorial radius a , polar radius c , and true oblateness $\epsilon = (a - c)/a$. Given it is a Maclaurin body, the apparent semi-major axis will be equal to the true semi-major axis ($a' = a$). In addition, we assume that it was observed with the same aspect angle θ during all the stellar occultations, which $\theta = 0^\circ$ (resp. 90°) corresponds to a pole-on (resp. equator-on) viewing. The maximum true oblateness that a Maclaurin object can have is $\epsilon \leq 0.417$ (Tancredi and Favre 2008), which gives $c = 234$ km. On the other hand, $c > 387$ km if we consider the $\epsilon = \epsilon' = 0.034$, derived from the occultation, as the lower limit for the object's true oblateness. If the above-mentioned conditions are true, those values for the pole radius can be understood as the minimum and maximum values.

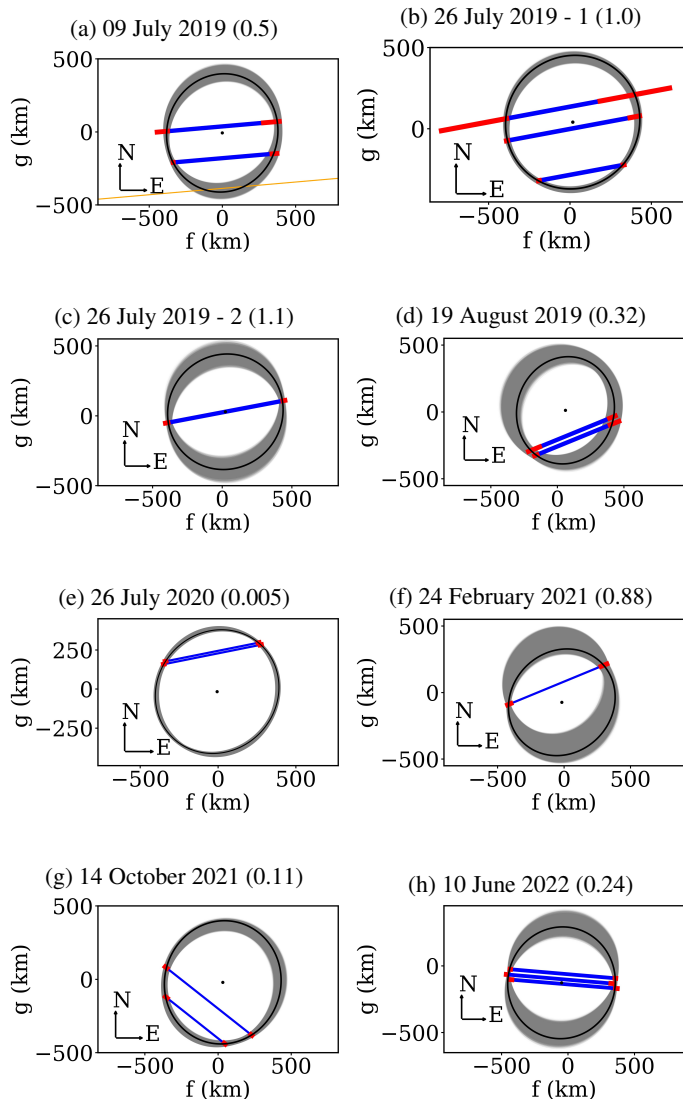


Fig. 8: Results for the additional eight stellar occultation events. Blue segments are the positive detections with 1σ uncertainties in red. The best elliptical limb is in black, with the center presented by the black dot. The gray region presents all the limb solutions within 3σ . The χ^2_{pdf} of each fit is presented between parenthesis in the individual labels. For the occultations presented in d, e, and f, the chosen center solution was the closest one to the predicted by NIMA v9 ephemeris.

The Maclaurin spheroid formalism (Braga-Ribas et al. 2013) allows us to estimate an object’s density from the true oblateness and rotational period. Using the lower limit of true oblateness from the occultation and the two rotational periods in the literature, we obtained an upper limit for global density of 8.0 g.cm^{-3} and 3.9 g.cm^{-3} for periods of 7.33 h and 10.44 h, respectively. These values are too high for objects in the trans-Neptunian region, so it is reasonable to infer that the true oblateness is higher than the observed in the stellar occultation events. As shown in Fig. 9, the density decreases as the true oblateness increases. Therefore, we can use the upper limit for the oblateness of a Maclaurin object ($\epsilon = 0.417$) to obtain the lower limits of MS₄’s global density, which gives 0.72 g.cm^{-3} and 0.36 g.cm^{-3} for 7.44 h and 10.44 h, respectively.

Finally, a geometric albedo of $p_V = 0.1 \pm 0.025$ was calculated using the equivalent radius from the occultation and the absolute magnitude on V-band of $H_V = 3.63 \pm 0.05 \text{ mag}$, which was obtained from the published V-magnitudes by Verbiscer et al. (2022). The obtained absolute magnitude is in agreement with (Tegler et al. 2016). However, we consider the different phase angles of the measurements and the error bar was calculated considering the expected amplitude of the rotational light curve of $\Delta_m = 0.05 \text{ mag}$ (Thirouin 2013; Thirouin et al. 2013).

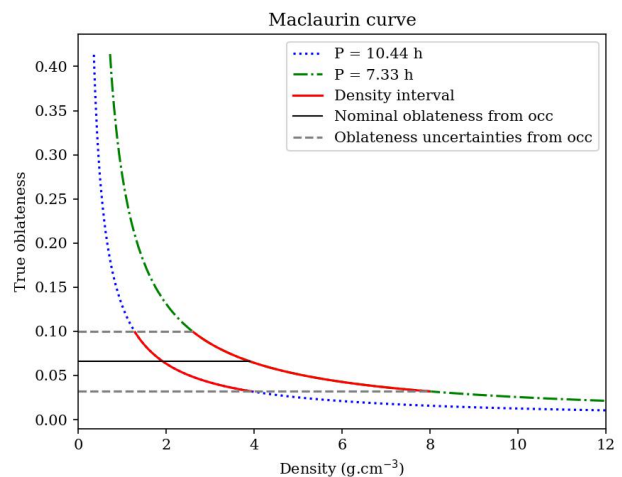


Fig. 9: Relation between the true oblateness and the density of a Maclaurin spheroid for the rotational periods of 10.44 h (blue dotted line) and 7.33 h (green dashed line). The solid black line is the nominal oblateness value with uncertainties (gray dashed lines) derived from the multichord stellar occultation event. Red segments present the global density interval for each rotational period assuming that the apparent oblateness corresponds to the real one.

4. Discussion and conclusions

This work presents physical and astrometric information derived from nine stellar occultations by the hot classical TNO (307261) 2002 MS₄ observed between 2019 and 2022 from South and North America, Africa, Europe, and Western Asia sites. The most successful campaign took place on 8 August 2020, with 116 telescopes involved and 61 positive chords, which represents a record number of detections of a stellar occultation by a TNO up to date.

The projected elliptical limb of MS₄ derived from the 8 August 2020 provides a semi-major axis of $412 \pm 10 \text{ km}$, a semi-minor axis of $385 \pm 17 \text{ km}$, and an area-equivalent radius of $398 \pm 12 \text{ km}$. The obtained diameter is $\approx 138 \text{ km}$ smaller than that derived with observations in thermal bands (Vilenius et al. 2012). It may indicate the presence of an unknown satellite as suggested for 2002 TC₃₀₂ in similar circumstances (Ortiz et al. 2020a). Still, the error bars from the thermal diameter are large and can accommodate the difference within 3σ .

Despite their being inconclusive, a shallow rotational light curve, the derived equivalent diameter, and the agreement between the limb obtained from the nine stellar occultations favor an oblate spheroid (Maclaurin) for the 3D shape of MS₄. Furthermore, considering the expected values for TNOs, the density intervals mentioned above are quite large. This indicates that the

object's true oblateness is higher than observed in the occultations or that the observed topography is the cause of the brightness variation in the rotational light curves. In the last case, the real rotational period may be double the published values, which provides smaller densities in the Maclaurin curve (Fig. 9). In any case, more data are needed to confirm MS4's 3D shape and density.

In addition, this work presents the first detailed multichord detection of an extensive feature on the surface of a monolithic TNO. A method was developed to identify and measure such detection. In the northeast region of the observed limb, a ≈ 11 km depth depression was found, followed by an elevation of 25_{-5}^{+4} km, subsequently followed by the most impressive feature, namely, a 45.1 ± 1.5 km depth depression with a linear extension of 322 ± 39 km. Assuming a straight line that connects the model's initial and endpoints, the largest feature has $\approx 40\%$ of the object's equivalent diameter. Such large topography is out of the range of expected global topography (Sect. 3.2) and may indicate a big impact during MS4 history. If so, one hypothesis that can be raised is whether the impact could have created a collisional family, such as that of Haumea (Brown et al. 2007; Vilenius et al. 2018), the only known collisional family in the trans-Neptunian region.

A comparison can be made with known craters in the outer Solar System. Among the largest Saturnian satellites, the Voyager and Cassini missions were able to acquire images of Tethys and Iapetus. The largest imaged craters are similar in size ratio to the feature observed in MS4. The Odysseus crater has a rim-to-rim diameter corresponding to $\approx 43\%$ of the Tethys's mean diameter. The Turgis¹² crater has a diameter of $\approx 40\%$ Iapetus' mean diameter (Moore et al. 2004; Thomas and Dermott 1991). However, the most recent and detailed studies about the surface of similar-to-MS4 objects in the trans-Neptunian region were performed for the Pluto-Charon system. Contrary to Saturn's satellites, the largest craters imaged by New Horizons have only 10.5% and 18.9% of the Pluto- and Charon-equivalent diameters, respectively (Moore et al. 2016). Therefore, the putative crater on the MS4 limb is the largest observed in the trans-Neptunian region, despite having a similar size ratio to craters found on planetary satellites.

Finally, even with the unprecedented coverage of a stellar occultation by a TNO, no clear secondary drops in the star flux caused by rings, jets, or satellites were identified. Establishing upper limits for detecting such structures in the occultation light curves is beyond the scope of this work. In addition, although it is still very unlikely, we cannot rule out the hypothesis that the elevation observed between $PA = 0^\circ$ and $PA = 25^\circ$ was caused by an unknown satellite with a diameter of ≈ 213 km passing in front of or behind the main body. If so, the main body would then have an effective diameter of ≈ 788 km (see Appendix D).

Acknowledgements. This study was financed in part by the Coordenação de Aperfeiçoamento de Pessoal de Nível Superior – Brazil (CAPES) – Finance Code 001, the National Institute of Science and Technology of the e-Universe project (INCT do e-Universo, CNPq grant 465376/2014-2), the Spanish MICIN/AEI/10.13039/501100011033, the Institute of Cosmos Sciences University of Barcelona (ICCUB, Unidad de Excelencia "María de Maeztu") through grant CEX2019-000918-M, the "ERDF A way of making Europe" by the "European Union" through grant PID2021-122842OB-C21, and within the "Lucky Star" umbrella that agglomerates the efforts of the Paris, Granada, and Rio teams, which the European Research Council funds under the European Community's H2020 (ERC Grant Agreement No. 669416). The following authors acknowledge the respective CNPq grants: F. L. R. 103096/2023-0; F.B.-R. 314772/2020-0; R.V.-M. 307368/2021-1; J.I.B.C. 308150/2016-3 and 305917/2019-6; M.A.

427700/2018-3, 310683/2017-3, 473002/2013-2; G. M. 128580/2020-8; B.E.M. 150612/2020-6; and O.C.W. 305210/2018-1. The following authors acknowledge the respective grants: B.E.M. thanks the CAPES/Cofecub-394/2016-05; G. M. thanks the CAPES grant 88887.705245/2022-00; G.B.-R. acknowledges CAPES - FAPERJ/PAPDRJ grant E26/203.173/2016 and the scholarship granted in the scope of the Program CAPES-PrInt, process number 88887.310463/2018-00, Mobility number 88887.571156/2020-00; M.A. acknowledges FAPERJ grant E-26/111.488/2013; A.R.G.Jr acknowledges FAPESP grant 2018/11239-8; O.C.W. and R.S. acknowledges FAPESP grant 2016/24561-0; K. B. acknowledges the scholarship funded by F.R.S.-FNRS grant T.0109.20 and by the Francqui Foundation; D.N. acknowledges the support from the French Centre National d'Etudes Spatiales (CNES); D. S. thanks to Fulbright Visiting Scholar (2022 - 2023) at the University of California, Berkeley; A.P. and R.S. thanks to the National Research, Development and Innovation Office (NKFIH, Hungary) grants K-138962 and K-125015. Partial funding for the computational infrastructure and database servers is received from the grant KEP-7/2018 of the Hungarian Academy of Sciences; R. D., J.L.O., P. S.-S., N. M., R. H., A. S. L., and J. M. T.-R. acknowledge the MICIN/AEI/10.13039/501100011033 under the grant respective grants: CEX2021-001131-S, PID2019-109467GB-I00, and PID2021-128062NB-I00; T. S. R. acknowledges funding from the NEO-MAPP project (H2020-EU-2-1-6/870377); K.H. was supported by the project R.V.O.: 67985815; A. K. thanks to the IRAP, Midi-Pyrenees Observatory, CNRS, University of Toulouse, France; J. M. O. acknowledges the Portuguese Foundation for Science and Technology (FCT) and the European Social Fund (ESF) through the Ph.D. grant SFRH/BD/131700/2017; J.d.W. and MIT acknowledge the Heising-Simons Foundation, Dr. and Mrs. Colin Masson, and Dr. Peter A. Gilman for Artemis, the first telescope of the SPECULOOS network situated in Tenerife, Spain. The ULiege's contribution to SPECULOOS has received funding from the ERC under the European Union's Seventh Framework Programme (FP/2007-2013) (grant number 336480/SPECULOOS); J. L. acknowledges the ACIISII, Consejería de Economía, Conocimiento y Empleo del Gobierno de Canarias, and the European Regional Development Fund (ERDF) under the grant PRID2021010134, also the Agencia Estatal de Investigación del Ministerio de Ciencia e Innovación (AEI-MCINN) under the grant PID2020-120464GB-I00; D. T., R. K., M. H., and T. P. were supported by the Slovak Grant Agency for Science grants number VEGA 2/0059/22, and VEGA 2/0031/22"; M. P. was supported by a grant from the Romanian National Authority for Scientific Research – UEFISCDI, project number PN-III-P1-1.1-TE-2019-1504; P. B., M. M., and M. D. G. thanks the support of the Italian Amateur Astronomers Union (UAI). This work has made use of data from the European Space Agency (ESA) mission *Gaia* (<https://www.cosmos.esa.int/gaia>), processed by the *Gaia* Data Processing and Analysis Consortium (DPAC, <https://www.cosmos.esa.int/web/gaia/dpac/consortium>). Funding for the DPAC has been provided by national institutions, in particular, the institutions participating in the *Gaia* Multilateral Agreement. The Joan Oró Telescope (TJO) of the Montsec Observatory (OdM) is owned by the Catalan Government and operated by the Institute for Space Studies of Catalonia (IEEC). TCH telescope is financed by the Island Council of Ibiza. IST60 and IST40 are the observational facilities of the Istanbul University Observatory, funded by the Scientific Research Projects Coordination Unit of Istanbul University with project numbers BAP-3685 and FBG-2017-23943 and the Presidency of Strategy and Budget of the Republic of Turkey with the project 2016K12137. TRAPPIST is a project funded by the Belgian FNRS grant PDR T.0120.21 and the ARC grant for Concerted Research Actions, financed by the Wallonia-Brussels Federation. E.J. is an FNRS Senior Research Associate. TRAPPIST-North is funded by the University of Liège and performed in collaboration with the Cadi Ayyad University of Marrakesh. This work made use of observations obtained at the 1.6 m telescope on the Pico dos Dias Observatory of the National Laboratory of Astrophysics (LNA/Brazil), at the Copernicus and Schmidt telescopes (Asiago, Italy) of the INAF-Astronomical Observatory of Padova, and at the Southern Astrophysical Research (SOAR) telescope, which is a joint project of the Ministério da Ciência, Tecnologia, e Inovação (MCTI) da República Federativa do Brasil, the U.S. National Optical Astronomy Observatory (NOAO), the University of North Carolina at Chapel Hill (UNC), and Michigan State University (MSU). We thank the following observers who participated and provided data for the events listed in Appendix A: A. Ciarella, A. L. Ivanov, A. Olsen, A. Ossola, B. Dintinjana, B. Hanna, C. Costa, G. H. Rudnick, J. Paul, J. J. Castellani, J. Polak, K. Guhl, L. A. Molnar, L. Perez, M. Bertini, M. Bigi, M. Rottenborn, M. Sabil, N. V. Ivanova, P. Langill, P. Thierry, S. Bouquillon, S. Lamina, T. O. Dementiev, V. A. Ivanov, and X. Delmotte.

References

Assafin, M., Vieira Martins, R., Camargo, J. I. B., et al.: 2011, *Gaia follow-up network for the Solar System objects: Gaia FUN-SSO workshop proceedings*, 85-88.

¹² Turgis diameter was obtained from <https://planetarynames.wr.usgs.gov/Feature/14488>.

- Assafin, M. 2023, PRAIA - Package for the Reduction of Astronomical Images Automatically. I. Photometry task, Astronomy, and Computing, submitted.
- Astropy Collaboration, Robitaille, T. P., Tollerud, E. J., et al.: 2013, *Astronomy & Astrophysics*, 558, A33. doi:10.1051/0004-6361/201322068
- Benecchi, S. D., Porter, S. B., Buie, M., et al.: 2019, *Icarus*, 334, 11.
- Braga-Ribas, F., Sicardy, B., Ortiz, J. L., et al.: 2013, *The Astrophysical Journal*, 773, 26.
- Braga-Ribas, F., Crispim, A., Vieira-Martins, et al.: 2019, *Journal of Physics Conference Series*, 1365, 012024. doi:10.1088/1742-6596/1365/1/012024.
- Brown, M.E., Barkume, K.M., Ragozzine, D., et al.: 2007, *Nature*, 446, 294. doi:10.1038/nature05619.
- Buie, M. W., Porter, S. B., Tamblyn, P., et al.: 2020, *The Astronomical Journal*, 159, 130. doi:10.3847/1538-3881/ab6ced.
- Butcher, H., Stevens, R. 1981, *Kitt Peak National Observatory Newsletter*, 16, 6.
- Chandrasekhar, S.: 1987, *New York : Dover*.
- Copejans, R., Gulbis, A.A.S., Kotze, et al.: 2013, *Publications of the Astronomical Society of the Pacific*, 125, 976. doi:10.1086/672156.
- Desmars, J.: 2015, *Astronomy & Astrophysics*, 575, A53. doi:10.1051/0004-6361/201423685.
- Desmars, J., Camargo, J.I.B., Braga-Ribas, F., et al.: 2015, *Astronomy & Astrophysics*, 584, A96. doi:10.1051/0004-6361/201526498.
- Dias-Oliveira, A., Sicardy, B., Ortiz, J. L., et al.: 2017, *The Astronomical Journal*, 154, 22.
- Foreman-Mackey, D., Hogg, D. W., Lang, D., et al.: 2013, *Publications of the Astronomical Society of the Pacific*, 125, 306. doi:10.1086/670067.
- Gaia Collaboration, Prust, T., de Bruijne, J. H. J., et al.: 2016 (a), *Astronomy & Astrophysics*, 595, A1.
- Gaia Collaboration, Brown, A. G. A., Vallenari, A., et al.: 2016 (b), *Astronomy & Astrophysics*, 595, A2.
- Gaia Collaboration, Brown, A. G. A., Vallenari, A., et al.: 2018, *Astronomy & Astrophysics*, 616, A1.
- Gaia Collaboration, Vallenari, A., et al.: 2023, *Astronomy & Astrophysics*, 674, A1. doi:10.1051/0004-6361/202243940.
- Gladman, B., Marsden, B. G., and Vanlaerhoven, C.: 2008, *The Solar System Beyond Neptune*, 43.
- Gomes-Júnior, A. R., Morgado, B. E., Benedetti-Rossi, G., et al.: 2022, *Monthly Notices of the Royal Astronomical Society*, 511, 1167. doi:10.1093/mnras/stac032.
- Jewitt, D., and Luu, J.: 1993, *Nature*, 362, 730.
- Jewitt, D., Morbidelli, A., and Rauer, H.: 2008, *Saas-Fee Advanced Course 35: Trans-Neptunian Objects and Comets*.
- Johnson, T.V. and McGetchin, T.R.: 1973, *Icarus*, 18, 612. doi:10.1016/0019-1035(73)90064-X.
- Kervella, P., Thévenin, F., Di Folco, E., et al.: 2004, *Astronomy & Astrophysics*, 426, 297. doi:10.1051/0004-6361:20035930.
- Kilic, Y., Braga-Ribas, F., Kaplan, M., Erece, O., et al.: 2022, *Monthly Notices of the Royal Astronomical Society*, 515, 1346. doi:10.1093/mnras/stac1595.
- Lacerda, P., Fornasier, S., Lellouch, E., et al.: 2014, *The Astrophysical Journal*, 793, L2. doi:10.1088/2041-8205/793/1/L2.
- Leiva, R., Sicardy, B., Camargo, J.I.B., et al.: 2017, *The Astronomical Journal*, 154, 159. doi:10.3847/1538-3881/aa8956.
- Lellouch, E., Santos-Sanz, P., Lacerda, P., et al.: 2013, *Astronomy & Astrophysics*, 557, A60.
- Loveless, S., Prialnik, D., and Podolak, M.: 2022, *The Astrophysical Journal*, 927, 178. doi:10.3847/1538-4357/ac4962.
- Moore, J.M., Schenk, P.M., Bruesch, L.S., et al.: 2004, *Icarus*, 171, 421. doi:10.1016/j.icarus.2004.05.009.
- Moore, J.M., McKinnon, W.B., Spencer, J.R., et al.: 2016, *Science*, 351, 1284. doi:10.1126/science.aad7055.
- Morbidelli, A., Levison, H. F., and Gomes, R.: 2008, *The Solar System Beyond Neptune*, 275.
- Müller, T., Lellouch, E., and Fornasier, S.: 2020, *The Trans-Neptunian Solar System*, 153.
- Nesvorný, D., and Morbidelli, A.: 2012, *The Astronomical Journal*, 144, 117.
- Nimmo, F., Umurhan, O., Lisse, C. M., et al.: 2017, *Icarus*, 287, 12. doi:10.1016/j.icarus.2016.06.027
- Ortiz, J.L., Santos-Sanz, P., Sicardy, B., et al.: 2020 (a), *Astronomy and Astrophysics*, 639, A134. doi:10.1051/0004-6361/202038046.
- Ortiz, J.L., Sicardy, B., Camargo, J. I. B., et al.: 2020 (b), *The Trans-Neptunian Solar System*, 413. doi:10.1016/B978-0-12-816490-7.00019-9.
- Pavlov, H., Anderson, R., Barry, T., et al.: 2020, *Journal for Occultation Astronomy*, 10, 8. doi:www.iota-es.de/JOA/JOA2020_3.pdf#page=8.
- Petit, J.-M., Kavelaars, J. J., Gladman, B., and Loredó, T.: 2008, *The Solar System Beyond Neptune*, 71.
- Schenk, P. M., and Moore, J. M.: 2020, *Philosophical Transactions of the Royal Society of London Series A*, 378, 20200102. doi:10.1098/rsta.2020.0102.
- Spencer, J. R., Stern, S. A., Moore, J. M., et al.: 2020 (a), *Science*, 367, aay3999.
- Spencer, J., Grundy, W. M., Nimmo, F., et al.: 2020 (b), *The Trans-Neptunian Solar System*, 271. doi:10.1016/B978-0-12-816490-7.00012-6.
- Stansberry, J., Grundy, W., Brown, M., et al.: 2008, *The Solar System Beyond Neptune*, 161.
- Stern, S. A., Bagenal, F., Ennico, K., et al.: 2015, *Science*, 350, aad1815. doi:10.1126/science.aad1815.
- Stern, S. A., Weaver, H. A., Spencer, J. R., et al.: 2019, *Science*, 364, aaw9771.
- Storn, R., and Price, K.: 1997, *Differential Evolution – A Simple and Efficient Heuristic for global Optimization over Continuous Spaces*, 11. doi.org/10.1023/A:1008202821328.
- Stern, S. A., Spencer, J. R., Verbiscer, A., et al.: 2020, *The Trans-Neptunian Solar System*, 379. doi:10.1016/B978-0-12-816490-7.00017-5.
- Tancredi, G., and Favre, S.: 2008, *Icarus*, 195, 851. doi:10.1016/j.icarus.2007.12.020.
- Tegler, S.C., Romanishin, W., Consolmagno, G.J., et al.: 2016, *The Astronomical Journal*, 152, 210. doi:10.3847/0004-6256/152/6/210.
- Thirouin, A., 2013. Study of Trans-Neptunian Objects using photometric techniques and numerical simulations. *Ph.D. Thesis*, ISBN: 978-84-9028-749-1.
- Thirouin, A., Noll, K.S., Campo Bagatin, A., Ortiz Moreno, J.L., and Morales, N.: 2013, *AAS/Division for Planetary Sciences Meeting Abstracts #45*.
- Thomas, P.C., and Dermott, S.F.: 1991, *Icarus*, 94, 391. doi:10.1016/0019-1035(91)90236-M.
- Van Laerhoven, C., Gladman, B., Volk, K., et al.: 2019, *The Astronomical Journal*, 158, 49. doi:10.3847/1538-3881/ab24e1.
- Verbiscer, A.J., Helfenstein, P., Porter, S.B., et al.: 2022, *The Planetary Science Journal*, 3, 95. doi:10.3847/PSJ/ac63a6.
- Vilenius, E., Kiss, C., Mommert, M., et al.: 2012, *Astronomy and Astrophysics*, 541, A94.
- Vilenius, E., Stansberry, J., Müller, T., et al.: 2018, *Astronomy and Astrophysics*, 618, A136. doi:10.1051/0004-6361/201732564.
- Weaver, H. A., and Stern, S. A.: 2008, *The Solar System Beyond Neptune*, 557.

¹ National Observatory/MCTI, R. General José Cristino 77, CEP20921-400, Rio de Janeiro, Brazil
e-mail: flaviarommel@on.br

² Interinstitutional e-Astronomy Laboratory - LInEA & INCT do e-Universo, Rio de Janeiro, Brazil

³ Federal University of Technology - Paraná (UTFPR - Curitiba), Av. Sete de Setembro 3165, Curitiba, Paraná, Brazil

⁴ Institute of Astrophysics of Andalucía, IAA-CSIC, Glorieta de la Astronomía s/n, 18008 Granada, Spain

⁵ LESIA, Paris Observatory, PSL University, CNRS, Sorbonne University, Univ. Paris Diderot, Sorbonne Paris Cité, 5 place Jules Janssen, 92195 Meudon, France

⁶ Polytechnic Institute of Advanced Sciences-IPSA, 63 boulevard de Brandebourg, 94200 Ivry-sur-Seine, France

⁷ Institute of Celestial Mechanics and Ephemeris Calculation (IM-CCE), Paris Observatory, PSL Research University, CNRS, Sorbonne University, UPMC Univ Paris 06, Univ. Lille, 77, Av. Denfert-Rochereau, 75014 Paris, France

⁸ Valongo Observatory, Federal University of Rio de Janeiro (UFRJ), Ladeira Pedro Antônio 43 - Saúde, 20080-090 Rio de Janeiro, Brazil

⁹ Orbital Dynamics and Planetology Group, São Paulo State University (UNESP), Av. Aríberto Pereira da Cunha 333, Guaratinguetá, 12516-410 São Paulo, Brazil

¹⁰ Institute of Physics, Federal University of Uberlândia, Uberlândia, Minas Gerais, Brazil

¹¹ Florida Space Institute, University of Central Florida, 12354 Research Parkway, Partnership 1, Orlando, Florida, United States of America

¹² Space Telescope Science Institute, Baltimore, Maryland, United States of America

¹³ Department of Astronomy, and of Earth and Planetary Science, 501, Campbell Hall, University of California, Berkeley, California 94720, United States of America

¹⁴ naXys, Department of Mathematics, University of Namur, Rue de Bruxelles 61, 5000 Namur, Belgium

¹⁵ Domaine de la Blaque Observatory, 83670 Varages, France

¹⁶ San Pedro de Atacama Celestial Explorations (SPACE), Chicache 81, Ayllu de Solor, 1410000 San Pedro de Atacama, Chile

¹⁷ Panamanian Observatory in San Pedro de Atacama (OPSPA), Chile

¹⁸ Anarchist Mt. Observatory, British Columbia, Canada

¹⁹ STAR Institute, University of Liège, Allée du 6 août 19C, 4000 Liège, Belgium

- 20 Côte d’Azur University, CNRS, Observatoire de la Côte d’Azur, IRD, Géoazur, 250 rue Albert Einstein, Sophia Antipolis 06560 Valbonne, France
- 21 Côte d’Azur Observatory, Géoazur UMR 7329, 2130 Route de l’Observatoire, 06460 Caussols, France
- 22 University of Zagreb, Faculty of Electrical Engineering and Computing, Department of Applied Physics, Unska 3, 10000 Zagreb, Croatia
- 23 Centro Astronómico Hispano en Andalucía, Observatorio de Calar Alto, Sierra de los Filabres, 04550 Gérgal, Spain
- 24 Hvar Observatory, Faculty of Geodesy, University of Zagreb, Kačićeva 26, 10000 Zagreb, Croatia
- 25 Gemini Observatory / NSF’s NOIRLab, Casilla 603, La Serena, Chile
- 26 Konkoly Observatory, Research Centre for Astronomy and Earth Sciences (ELKH), H-1121 Budapest, Konkoly Thege Miklos út 15-17, Hungary
- 27 CSFK, MTA Centre of Excellence, Budapest, Konkoly Thege Miklós út 15-17, 1121 Hungary
- 28 Algiers Observatory, CRAAG, Route de l’Observatoire, Algiers, Algeria
- 29 Odesa I. I. Mechnikov National University, Astronomical Observatory, Marazliivska 1v, 65014 Odesa, Ukraine
- 30 Main astronomical observatory of National Academy of Sciences of Ukraine, 27 Akademika Zabolotnoho St., 03143 Kyiv, Ukraine
- 31 Department of Astronomy and Space Sciences, Faculty of Science, Istanbul University, 34116 Istanbul, Turkey
- 32 Istanbul University Observatory Research and Application Center, 34116 Istanbul, Turkey
- 33 Research Centre for Astronomy, Astrophysics and Astrophotonics, Department of Physics and Astronomy, Macquarie University, 2109, Sydney, Australia
- 34 ARC Centre of Excellence for All-Sky Astrophysics in 3 Dimensions (ASTRO 3D), Australia
- 35 Çanakkale Onsekiz Mart University, School of Graduate Studies, Department of Physics, 17100 Çanakkale, Turkey
- 36 Çanakkale Onsekiz Mart University, Astrophysics Research Center and Ulupınar Observatory, 17100 Çanakkale, Turkey
- 37 International Occultation Timing Association - European Section (IOTA-ES), Am Brombeerhag 13, 30459, Hannover, Germany
- 38 Sabadell Astronomical Association, Carrer Prat de la Riba, s/n, 08206 Sabadell, Catalonia, Spain
- 39 PSTJ astronomy club - CIV 190 Rue Frédéric Mistral, 06560 Valbonne, France
- 40 British Astronomical Association (BAA), England
- 41 AstroCampania, Italy
- 42 Instituto de Física Aplicada a las Ciencias y las Tecnologías, Alicante University, San Vicente del Raspeig, 03080 Alicante, Spain
- 43 Institut de Ciències del Cosmos (ICCUB), Barcelona University (IEEC-UB), Carrer de Martí i Franquès 1, 08028 Barcelona, Spain
- 44 Ponta Grossa State University, Av. Carlos Cavalcanti 4748, Ponta Grossa, Paraná, Brazil
- 45 Department of Earth, Atmospheric and Planetary Science, Massachusetts Institute of Technology, 77 Massachusetts Avenue, Cambridge, Massachusetts, United States of America
- 46 Astrobiology Research Unit, University of Liège, Allée du 6 août 19C, 4000 Liège, Belgium
- 47 Canary Islands Institute of Astrophysics (IAC), Vía Láctea s/n, 38205 La Laguna, Tenerife, Spain
- 48 INAF - Catania Astrophysical Observatory, via S. Sofia 78, 95123 Catania, Italy
- 49 Campo Catino Astronomical Observatory, Guarcino, Italy
- 50 Institute of Astronomy of V.N. Karazin Kharkiv National University, Kharkiv 61022, Sumska str. 35, Ukraine
- 51 Astronomical Observatory Institute, Faculty of Physics, Adam Mickiewicz University, Słoneczna 36, 60-286, Poznań, Poland
- 52 Črni Vrh Observatory, Predgrize 29A, 5274 Črni Vrh nad Idrijo, Slovenia
- 53 University of Ljubljana, Faculty of Mathematics and Physics, Jadranska 19, 1000 Ljubljana, Slovenia
- 54 Pistoiese Mountain Astronomical Observatory (GAMP), San Marcello Pistoiese, Italy
- 55 Astronomical Association of Eivissa (AAE), Lucio Oculacio 29, 07800 Ibiza, Spain
- 56 Monte Agliale Astronomical Observatory, Via Cune Motrone, 55023 Borgo a Mozzano, Italy
- 57 QOS Observatory, Center for Special Information Reception and Processing and Navigation Field Control, National Space Facilities Control and Test Center, Zalitsi village, 32444 Kamianets-Podilskyi district, Khmelnytskyi region, Ukraine
- 58 La Laguna University (ULL), Astrophysics department, Avenida Astrofísico Francisco Sánchez, s/n. Facultad de Ciencias. Sección de Física, 38200 La Laguna, Tenerife, Spain
- 59 Virtual Telescope Project, Via Madonna de Loco 47, 03023 Ceccano, Italy
- 60 G. Pascoli Observatory (MPC K63), Castelveccchio Pascoli, Italy
- 61 Red ASTRONAVARRA sarea, Spain
- 62 club Astrospace Thales Alenia Space, Cannes, France
- 63 University of Lille, Lille Observatory, 1 impasse de l’observatoire, 59000 Lille, France
- 64 Tavolaia Observatory (MPC A29), Santa Maria a Monte, Pisa, Italy
- 65 Romanian Society for Cultural Astronomy - SRPAC, Timisoara, Romania
- 66 EPT Observatories, Tijarafe, La Palma, Spain
- 67 Penticton Secondary School, 158 Eckhardt Ave East Penticton, British Columbia, Canada
- 68 OACM Observatory, Fuensanta de Martos, Jaen, Spain
- 69 Associazione Astrofili Fiorentini (A.A.F.) - Via Giulio Caccini, 13b, 50141 Firenze, Italy
- 70 Astronomical Society of Southern Africa, Centurion, South Africa
- 71 Nastro Verde Astronomical Observatory, Sorrento, Italy
- 72 Cosmos Observatory, Marbella, Spain
- 73 INAF - Trieste Astrophysical Observatory, via G. B. Tiepolo 11, 34143 Trieste, Italy
- 74 Lowell Observatory, Flagstaff, Arizona, United States of America
- 75 ROASTERR - 1 Observatory, Cluj-Napoca, Romania
- 76 PS Observatory (MPC M35), Bacau, Romania
- 77 The American Association of Variable Star Observers (AAVSO), 185 Alewife Brook Parkway, Suite 410, Cambridge, MA 02138, United States of America
- 78 ALMO Observatory via Forlai 14/C - 40010 Sala Bolognese, Bologna, Italy
- 79 UAI (Union of Italian Amateur Astronomers) c/o Osservatorio Astronomico “F. Fuligni” Via Lazio 14, 00040 Rocca di Papa, Roma, Italy
- 80 Telescope Live, 71-75 Shelton Street, Covent Garden, London, WC2H 9JQ, England
- 81 Bucharest Astroclub, Bd. Lascar Catargiu 21, 010662 Bucharest, Romania

- 82 Astronomical Society of Tunisia (SAT), Tunis, Tunisia
- 83 University of Tunis El Manar, University Campus Farhat Hached B.P. 94 Rommana, 1068 Tunis, Tunisia
- 84 Ad Astra Sangos Observatory (MPC Z07), Calle Hernán Cortés 4, Alhendín, Granada, Spain
- 85 Sociedad Astronómica Granadina, Granada, Spain
- 86 Stardust Observatory, Brasov, Romania
- 87 Bârlad Observatory, Bârlad, Romania
- 88 Astronomical Institute of the Romanian Academy, Bucharest, 5 Cuřitul de Argint, 040557 Bucharest, Romania
- 89 Tree Gate Farm Observatory, Mississippi, United States of America
- 90 Observer from South Africa
- 91 Syrma-GUA, Valladolid, Spain
- 92 Department of Space Sciences and Technologies, Akdeniz University, Campus, Antalya 07058, Turkey
- 93 TÜBİTAK National Observatory, Akdeniz University Campus, Antalya 07058, Turkey
- 94 Euraster, 8 rue du tonnelier, 46100 Faycelles, France
- 95 IRAP, Midi-Pyrenees Observatory, CNRS, University of Toulouse, BP 4346, 31028 Toulouse Cedex 04, France
- 96 Dax Observatory, rue Pascal Lafitte, 40100 Dax, France
- 97 El Leoncito Astronomical Complex, National Council for Scientific and Technical Research, San Juan, Argentina
- 98 National University of La Plata, Facultad de Ciencias Astronómicas y Geofísicas, Paseo del Bosque S/N—B1900FWA, La Plata, Argentina
- 99 National University of La Plata, Instituto de Astrofísica de La Plata (CCT La Plata - CONICET/UNLP), B1900FWA La Plata, Argentina
- 100 University Observatory, Ludwig-Maximilians, Munich University, Scheiner Str. 1, 81679 Munich, Germany
- 101 Astronomical Institute, Slovak Academy of Sciences, 05960 Tatranská Lomnica, Slovakia
- 102 G. V. Schiaparelli Astronomical Observatory, Campo dei Fiori, Varese, Italy
- 103 Observer from Munich, Germany
- 104 National Astrophysics Institute, Padova Astronomical Observatory, Vicolo dell'Osservatorio 5, 35122 Padova, Italy
- 105 Aix Marseille University, CNRS, CNES, LAM, Marseille, 13007, France
- 106 Astronomical Institute of the Czech Academy of Sciences, Friřcova 1, 25165 Ondřejov, Czech Republic
- 107 Adiyaman University, Department of Physics, 02040 Adiyaman, Turkey
- 108 Astrophysics Application and Research Center, Adiyaman University, Adiyaman 02040, Turkey
- 109 Ataturk University, Department of Astronomy and Space Science, Yakutiye, 25240, Erzurum, Turkey
- 110 Max-Planck-Institut für extraterrestrische Physik, Giessenbachstrasse, 85748 Garching, Germany
- 111 Sybilla Technologies, Torunska 59, 85-023 Bydgoszcz, Poland
- 112 Mt. Suhora Observatory, Pedagogical University of Cracow, Podchorazych 2, 30-086 Cracow, Poland
- 113 Polytechnic Institute of Tomar, Ci2-Smart Cities Research Center and Unidade Departamental de Matemática e Física (UDMF), 2300 Tomar, Portugal
- 114 Aristotle University of Thessaloniki (AUTH), 54124, Greece
- 115 Centro Ciência Viva de Constância-Parque de Astronomia, Alto de Santa Bárbara, Via Galileu Galilei 817, 2250-100 Constância, Portugal
- 116 Buelach Observatory (MPC 167), Switzerland
- 117 Stellar Occultation Timing Association Switzerland (SOTAS), Swiss Astronomical Society, Switzerland
- 118 Türksat Observatory - Türksat Company Headquarters Campus, Gölbaşı, Ankara, Turkey
- 119 Çukurova University, Department of Astronomy and Astrophysics, Çukurova Üniversitesi Rektörlüğü, 01330 Sarıçam/Adana, Turkey
- 120 Adana Yuregir Science Center and Mesopotamia Astronomy Association, Adana, Turkey
- 121 Teplice Observatory, North-Bohemian Observatory and Planetarium in Teplice, Koperníkova 3062, 41501 Teplice, Czech Republic
- 122 Zákopčie, Čadca, Slovakia
- 123 GiaGa Observatory, Pogliano Milanese, Milan, Italy
- 124 Observer from Bolzano, Italy
- 125 Amateur Astronomical Observatory of Seysses, Seysses, France
- 126 The Pleiades Latrape Observatory, Grand Rue, 31310 Latrape, France
- 127 Herne Observatory, Am Böckenbusch 2a, 44652 Herne, Germany
- 128 Board of Polish Amateur Astronomers Society - Krakow, Poland
- 129 Polish Astronomical Society, Warsaw, Poland
- 130 Observer from Księżyno, Poland
- 131 French Astronomical Society (SAF), France
- 132 KYSUCE Observatory (MPC G02), Kysucke Nove Mesto, Slovakia
- 133 Czech Astronomical Society, Czech Republic
- 134 Observatory in Rokycany and Pilsen, Voldušská 721, 33701 Rokycany, Czech Republic
- 135 ADAGIO Association, Belestá Observatory (MPC A05), Toulouse, France
- 136 El Gato Gris Astronomical Observatory (MPC I19), Tanti, Córdoba, Argentina
- 137 Grupo de Observadores de Rotaciones de Asteroides (GORA), Argentina
- 138 Proyecto de Observación Colaborativa y Regional de Ocultaciones Asteroidales (POCROA), Argentina
- 139 El Catalejo Observatory (MPC I48), Santa Rosa, La Pampa, Argentina
- 140 Planetary Science Institute, 1700 East Fort Lowell Road, Suite 106, Tucson, Arizona 85719, United States of America
- 141 Applied Physics, Bilbao School of Engineering, University of País Vasco, UPV/EHU, Bilbao, Spain
- 142 University of Oregon, Eugene, Oregon, United States of America
- 143 Purdue University Northwest, Department of Chemistry and Physics, Hammond, Indiana, United States of America

- ¹⁴⁴ Vasile Urseanu Observatory, Bucharest, Romania
- ¹⁴⁵ Eskişehir Technical University, Astrophysical Education and Research Unit, Yunusemre Observatory, Eskişehir, Turkey
- ¹⁴⁶ Section of Astrophysics, Astronomy and Mechanics, Department of Physics, National and Kapodistrian University of Athens, 15784 Zografos, Athens, Greece
- ¹⁴⁷ Institut für Astronomie und Astrophysik, Eberhard Karls Universität Tübingen, Auf der Morgenstelle 10, 72076 Tübingen, Germany
- ¹⁴⁸ Ondokuz Mayıs University, Samsun, Turkey
- ¹⁴⁹ Institute of Space Sciences (CSIC-IEEC), Campus UAB, Carrer de Can Magrans s/n, 08193 Cerdanyola del Vallès, Catalonia, Spain
- ¹⁵⁰ Sparta Astronomy Association, Sparta, Greece
- ¹⁵¹ NOAK Observatory (MPC L02), Ioannina, Greece
- ¹⁵² Department of Physics, University of Ioannina, Ioannina 45110, Greece
- ¹⁵³ Observer from Romania
- ¹⁵⁴ Los Cabezones Observatory (MPC X12), Santa Rosa, La Pampa, Argentina
- ¹⁵⁵ University of Idaho, Department of Physics, Stop 440903, Moscow, Idaho, 83843, United States of America
- ¹⁵⁶ Department of Space Studies, University of North Dakota, 4149 University Avenue Stop 9008, Grand Forks, North Dakota 58202-9008, United States of America
- ¹⁵⁷ Chagrin Valley Astronomical Society, 15701 Huntley Rd, Huntsburg, Ohio 44046, United States of America
- ¹⁵⁸ Astronomy Department, University of Chile, Camino del Observatorio 1515, Casilla 36-D, Las Condes, Santiago, Chile
- ¹⁵⁹ Centro de Excelencia en Astrofísica y Tecnologías Afines (CATA), Chile
- ¹⁶⁰ Millenium Institute of Astrophysics (MAS), Chile
- ¹⁶¹ Institute of Space Science, 409 Atomistilor Street Magurele, 077125 Ilfov, Romania
- ¹⁶² Squirrel Valley Observatory (MPC W34), Columbus, North Carolina, United States of America
- ¹⁶³ Department of Physics and Astronomy, University of North Carolina Asheville, 1 University Heights, Asheville, North Carolina 28804, United States of America

Appendix A: Post occultation maps with sites location

Here we present the post-occultation maps of each stellar occultation by 2002 MS₄ described in this work.

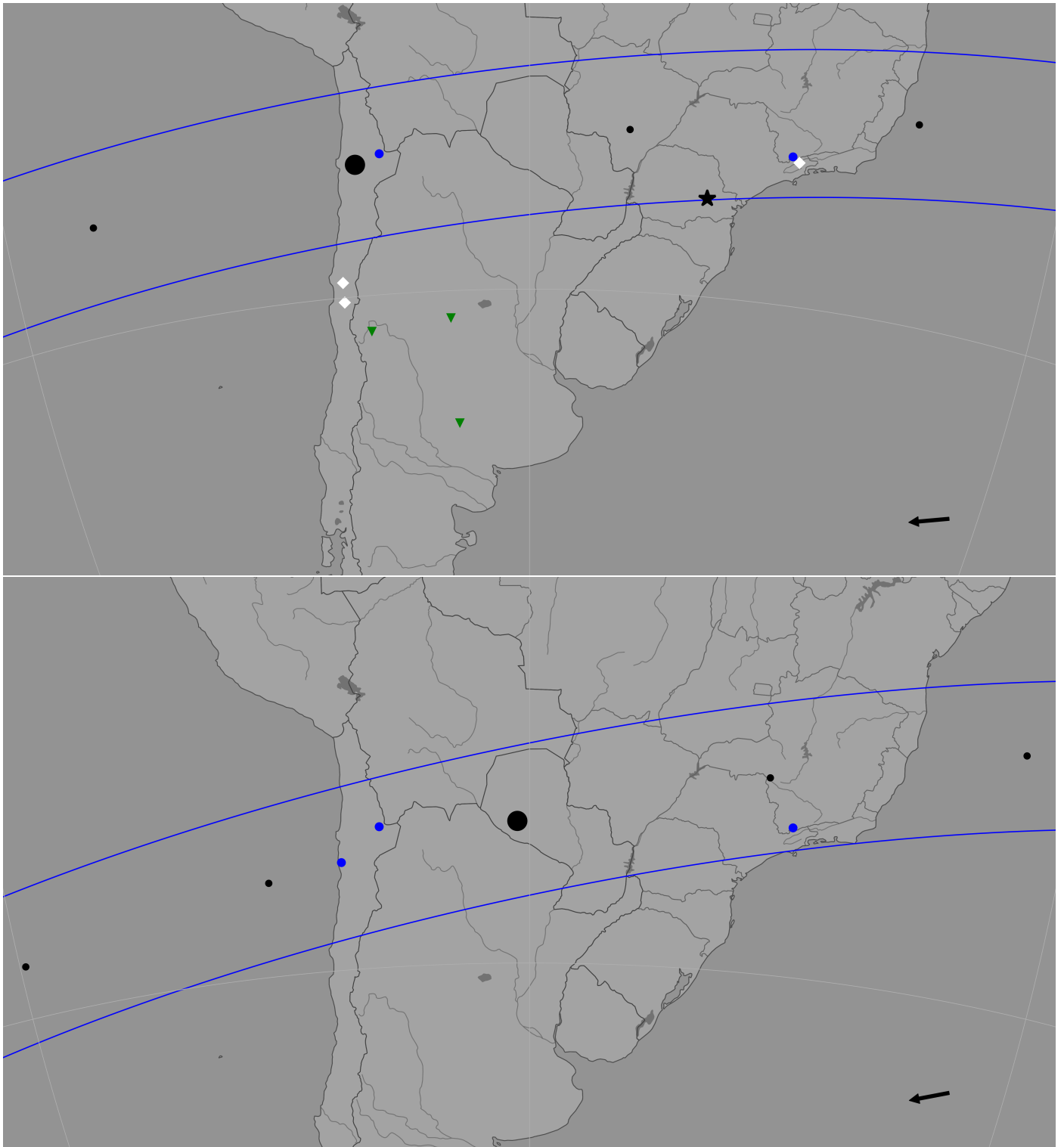


Fig. A.1: Post-occultation map of the stellar occultations observed on July 09 (upper panel) and July 26, 2019 (lower panel) from South America. Solid blue lines and black dots indicate the observed shadow path every minute, and the largest black bullet represents the closest approach instant. The arrow shows the shadow direction over Earth's surface. Blue dots show the positive detections, green triangles show the negatives, and white diamonds show the stations with bad weather conditions or technical problems. The black star marks the Ponta Grossa station, a close negative chord that limits the ellipse solutions at the south for the July 09, 2019, event.

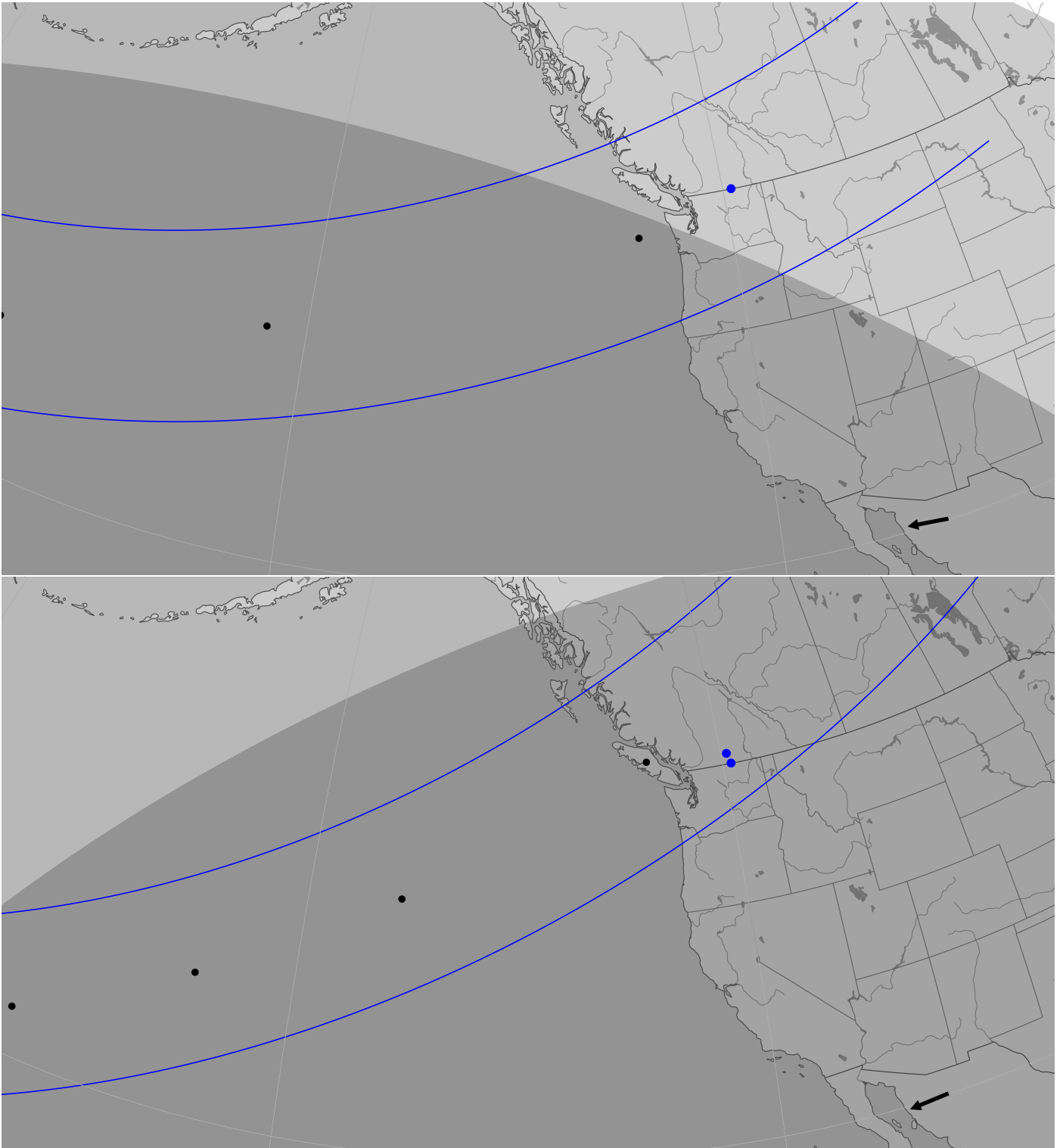


Fig. A.2: Post-occultation map of the stellar occultations observed on July 26 (upper panel) and August 19, 2019 (lower panel) from North America. Solid blue lines and black dots indicate the observed shadow path every minute. The arrow shows the shadow direction over Earth's surface, and the blue dots show the positive detections.

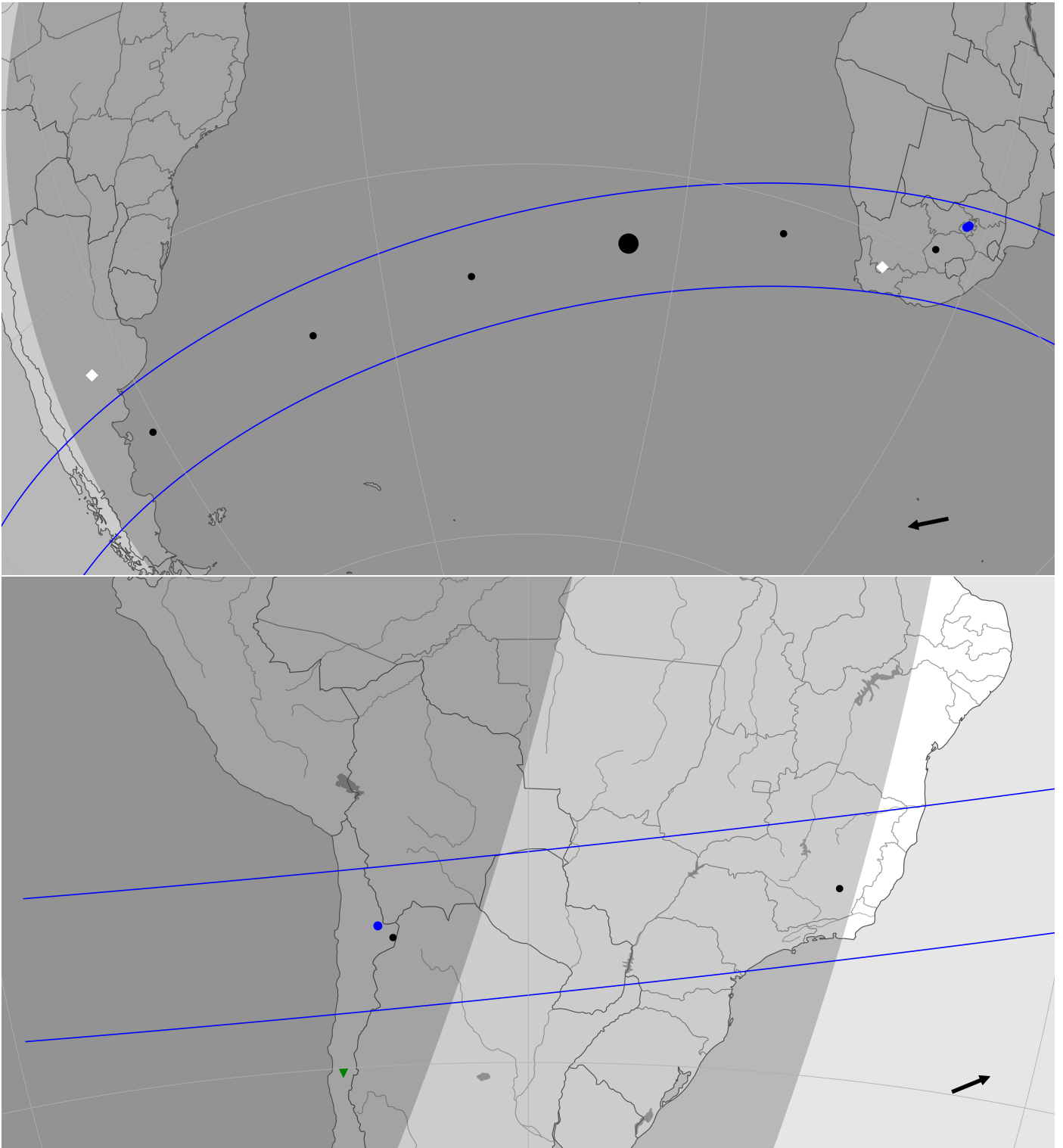


Fig. A.3: Post-occultation map of the stellar occultations observed on July 26, 2020, from South Africa and South America (upper panel) and on February 24, 2021, also from South America (lower panel). Solid blue lines and black dots indicate the observed shadow path every minute, and the largest black bullet represents the closest approach instant. The arrow shows the shadow direction over Earth's surface. Blue dots show the positive detections, green triangles show the negatives, and white diamonds show the stations with bad weather conditions or technical problems.

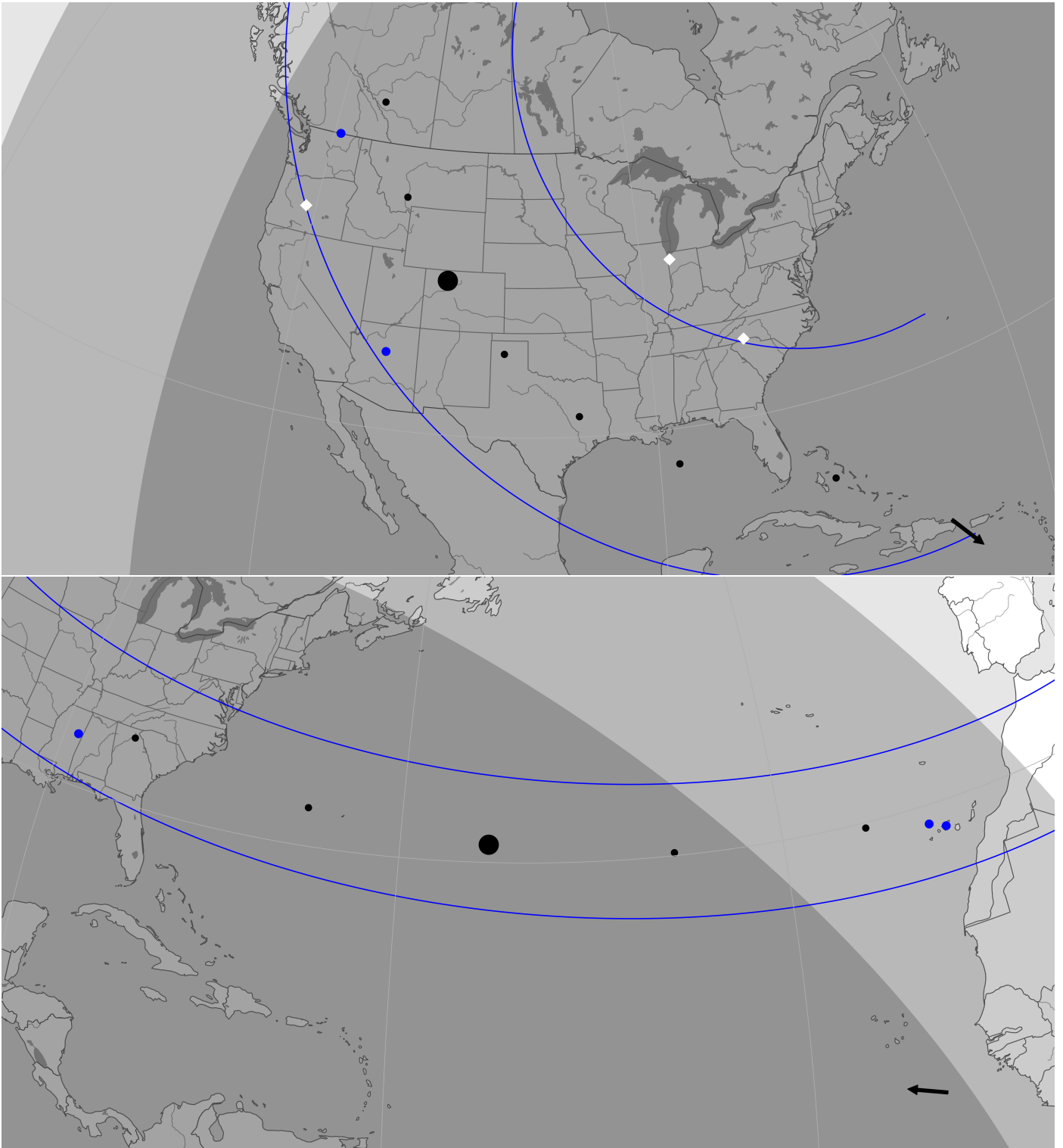


Fig. A.4: Post-occultation map of the stellar occultations observed on October 14, 2021, from North America (upper panel) and on June 10, 2022, from North America and Europe (lower panel). Solid blue lines and black dots indicate the observed shadow path every minute, and the largest black bullet represents the closest approach instant. The arrow shows the shadow direction over Earth's surface. Blue dots show the positive detections, and white diamonds show the stations with bad weather conditions or technical problems.

Appendix B: Observational circumstances

The following tables summarize the observational circumstances of each station of the nine stellar occultations presented in this work. For better visualization, the tables were divided into two groups i) the 8 August 2020 event and ii) the other eight stellar occultations. The positive, negative, and overcast locations involved in the 8 August 2020 campaign are listed in Tables B.1, B.2, and B.3, respectively. Positive and negative observations of the other eight events are present in Tables B.4 and B.5, respectively.

Table B.1: Observational circumstances of all observatories that detected the stellar occultation by MS₄ on 8 August 2020. The * symbol indicates that this data was taken in drift scan mode.

Observatory, nearest city, country	Latitude (°), longitude (°), altitude (m)	Telescope, aperture (m), filter	Time source, instrument	Exposure (s), cycle (s), correction (s)	Observers
Domaine de La Blaque, Varages, France	+43.61239 +05.96363 468.0	Ritchey-Chrétien 0.5 Clear	GPS WATEC 910HX	0.32 0.32 -	Jean Lecacheux, Jean-Luc Plouvier
TAROT Calern, Caussols, France	+43.752001 +06.923613 1268.0	TAROT North 0.25 Clear	GPS Andor DZ936N-BEX2-DD	90.0* 90.0* -	Eric Frappa, Alain Klotz
Méo Station, Grasse, France	+43.7546 +06.9216 1323.1	Ritchey-Chrétien 1.54 Clear	NTP ZWO ASI1600MM	1.0 1.0 -	Dominique Albanese, Hervé Mariey
Caussols, Caussols, France	+43.753055556 +6.921666667 1268.0	CFF T400 0.40 Clear	NTP ZWO 294 MC -	3.0 4.0 +0.4	Raymond Behem, Jean Pierre Prost
Sta Maria de Montmagastrell, Lleida, Spain	+41.720166 +01.105361 318.0	- 0.406 Clear	NTP SBIG STL-11000	7.0 18.0 -4.0	Josep M. Bosch Ignés
Saint-Paul-en-Forêt, Cannes, France	+43.560124 +06.962868 45.0	- 0.2 Clear	NTP ZWO ASI290MM	2.0 2.22 -	Romain Fafet
Nice, Nice, France	+43.725902 +07.299875 364.0	- 0.4 Clear	GPS Raptor Photonics	0.3 0.3 -3.7	Stéfan Renner, Matthieu Conjat
Valbonne, Valbonne, France	+43.619604 +07.039157 174.0	François Giraud (TFG) 0.4 Clear	GPS WATEC 910HX	1.0688 1.5163 -0.5339	Florian Signoret
Crni Vrh, Crni Vrh, Slovenia	+45.94586111 +14.07122222 726.0	Cichocki Sky Survey 0.6 W (clear)	NTP Apogee Alta U16M	1.5984 3.1095 -	Herman Mikuz
Pizskéstető Mountain Station, Mátraszentistván, Hungary	+47.917833 +19.8955833 960.0	Ritchey-Chrétien-Coudé 1.0 Clear	NTP Andor iXon - 888	0.56115 0.56791 -	Róbert Szakáts
University of Ljubljana, Ljubljana, Slovenia	+46.043806 +14.5274444 400.0	- 0.25 Clear	NTP QHY 5III-178M	2.0 2.0 -	Bojan Dintinjana
Konkoly Observatory, Budapest, Hungary	+47.4999553 +18.9620488 470.0	Refractor 0.3 Clear	NTP ASI178MM	1.0 1.0385 -	András Pál, Balázs Csák
Trieste, Trieste, Italy	+45.642721 +13.875383 400.0	Schmidt-Cassegrain 0.355 Luminance	NTP Apogee U Alta KAF-8300	4.0 5.0 +2.0	Paolo Di Marcantonio, Igor Coretti, Giulia Iafrate, Veronica Baldini
Sant Esteve Sesrovires, Catalonia, Spain	+41.494867 +01.8738 180.0	Newtonian 0.4 Clear	GPS Mintron 12V6HC-EX	1.28 1.28 -1.28	Carles Schnabel, Martí Schnabel
ALMO Observatory, Bologna (Padulle), Italy	+44.627 +11.2805 19.0	Schmidt-Cassegrain 0.235 Clear	NTP ZWO ASI120mm	3.0 3.0 +1.0	Adriano Valvasori, Ernesto Guido
- Massa, Italy	+44.026083333 +10.138611111 41.0	Schmidt-Cassegrain 0.2 Clear	GPS WATEC 910BD	2.56 2.60 -2.56	Michele Bigi
G. Pascoli, Castelvecchio Pascoli, Italy	+44.0603 +10.4625 257.0	Newtonian 0.41 Clear	NTP Sony QHY22	1.5 4.0 +2.2	Roberto Bacci

Table B.1 continued

Mount Agiale, Borgo a Mozzano, Italy	+43.99530 +10.51494 750.0	Newtonian 0.50 Clear	NTP FLI - Proline 4710	4.0 5.35 -	Fabrizio Ciabattari
Pistoiese Mountain, San Marcello Pistoiese, Italy	+44.063055 +10.804166 990.0	Newtonian 0.6 Clear	NTP (GPS-PPS) Apogee U6 Alta	1.0 3.13 -	Paolo Bacci, Martina Maestripieri, Marta Di Grazia
Tavolaia, Sta. Maria a Monte, Italy	+43.736833 +10.673445 34.0	Newtonian 0.4 Clear	NTP ASI 174 MM	2.0 2.0 -2.0	Mauro Bachini, Giacomo Succi
Spica, Signa, Italy	+43.789336 +11.089922 50.0	- 0.3 Clear	NTP SBIG ST-402 XME	3.0 4.0 -	Mauro Bertini
Margherita Hack, Lastra a Signa, Italy	+43.742280556 +11.1030305556 216.0	- 0.356 Clear	NTP SBIG ST10XME	2.0 4.45 -	Nico Montigiani, Massimiliano Mannucci
Zalistci, Khmelnyskiy, Ukraine	+48.84775 +26.72131 355.0	Newtonian 0.5 Clear	GPS FLI 16070	2.0 33.2 -	T. O. Dementiev, O. M. Kozhukhov
- Sevilla, Spain	+37.346111 -5.980556 28.0	- 0.28 Clear	GPS QHY 174M	0.6 0.6 -	Jose Maria Madiedo
El Arenosillo, Huelva, Spain	+37.103889 -06.7338889 54.0	BOOTES-1B 0.3 Clear	NTP Andor Ixon	2.0 4.0 -0.7	Emilio Jesus Fernández García, Alberto J. Castro Tirado
ROASTERR-1, Cluj-Napoca, Romania	+46.820954 +23.596400 390.0	- 0.3 Clear	NTP atik 383L+	4.0 5.0 -	Lucian Hudin
Fuensanta de Martos, Fuensanta de Martos, Spain	+37.646389 -03.917468 710.0	Newtonian 0.36 Luminance	atom time SBIG ST-10xme	2.0 8.0 -	Jose Carrillo Gomez
- Fiastra, Italy	+43.057093 +13.173074 700.0	- 0.254 Clear	NTP SBIG ST8-XME	3.0 6.1 -	Alessio Ciarella
- Dragsina, Romania	+45.703344 +21.436879 97.0	- 0.4 Clear	NTP ZWO ASI 1600MM-Pro	0.9 1.47 -2.0	Liviu Stoian, Andrei Juravle
Cala D'Hort, Ibiza, Spain	+38.89111111 -1.24083333 130.0	TCH 0.51 Luminance	NTP Sbig STL1000	3.0 6.0 -	Ignacio de la Cueva Torregrosa, Marco Yuste-Moreno
Alhendín, Granada, Spain	+37.1110313 -03.6394227 740.0	Newtonian 0.2 Clear	NTP ZWO ASI 178MM	5.0 5.125 -	Miguel Sánchez González
Sierra Nevada, Granada, Spain	+37.0641667 -03.384722 2896.0	T150 1.5 Clear	NTP Andor Ikon-L	1.0 2.0 -	Alfredo Sota, Pablo Santos Sanz, José Luis Ortiz, Nicolás Morales
Sierra Nevada, Granada, Spain	+37.0641667 -03.384722 2896.0	T90 0.9 Clear	NTP Roper VersArray	1.0 3.0 -	
Cancelada, Estepona, Spain	+36.461111111 -05.054444444 25.0	- 0.254 Luminance	Mount Sync MaxIm DL 6 ATIK - 460 ex	10.0 18.0 -	Juan Francisco Calvo Fernández
Cosmos, Marbella, Spain	+36.516229 -04.857376 70.0	- 0.355 Luminance	NTP ATIK 460ex	10.0 21.0 -	Fran Cuevas
Colle S. Agata, Rome, Italy	+41.9495555 +12.42855555 124.0	Schmidt-Cassegrain 0.28 Clear	GPS QHY174M	2.0 2.0 -	Claudio Costa
Hvar, Hvar, Croatia	+43.178944 +16.447748 190.0	- 1.06 Clear	NTP ASI294MC Pro	3.0 3.2 -	Stefan Cikota, Domagoj Ruždjak, Aleksandar Cikota
PS Observatory, Bacau, Romania	+46.50779 +26.80007 555.0	Newtonian 0.254 IR Cut	NTP ZWO ASI 178 MM	3.0 3.18 -	Radu Mihai Anghel

Table B.1 continued

Agrustos, Sassari, Italy	+40.7278448 +09.6948317 20.0	SC 0.13 Clear	GPS QHY174 M	4.0 4.0 -	Salvatore Lamina
Campo Catino, Guarcino, Italy	+41.821115 +13.3292867 1485.0	Ritchey-Chretien 0.8 Clear	GPS QHY 174C	1.0 1.0 -3.0	Ugo Tagliaferri, Mario Di Sora, Giovanni Isopi
Kharkiv University, Kharkiv, Ukraine	+49.64083 +36.93389 156.0	Reflector AZT - 8 0.7 Luminance	NTP FLI ML4710	2.0 3.0 -	Y. Krugly, I. Slyusarev, V. Chiorny
Kharkiv University, Kharkiv, Ukraine	+49.64083 +36.93389 156.0	Baker-Schmidt 0.36 R	NTP FLI PL1001E	4.0 5.0 -	Y. Krugly, A.Zheleznyak
Ceccano, Ceccano, Italy	+41.567717 +13.333301 178.0	- 0.432 Clear	NTP SBIG STL-6303E	3.5 4.0 -	Gianluca Masi
Stardust, Brasov, Romania	+45.641611 +25.621889 597.0	CPC800 0.2 Clear	NTP Atik 383L+	10.0 13.0 -	Lucian Curelaru
- Bârlad, Romania	+46.2313888 +27.6694444 70.0	EQMOD ASCOM 0.2 Luminance	NTP ASI 1600	8.0 8.8 -	Dumitru Ciprian Vîntdevară
Stardreams, Valenii de Munte, Romania	+45.203642 +26.045526 380.0	Ritchey-Chretien 0.203 Clear	NTP ATIK 460ex	4.0 5.0 +1.5	Radu Mihai Gherase
St. George, Ploiesti, Romania	+45.007213 +25.978711 243.0	- 0.19 Luminance	NTP ATIK 460EX mono	7.0 8.0 -18.0	Cristian Adrian Danescu
Odesa-Mayaki, Odesa, Ukraine	+46.39696195 +30.27127709 19.0	OMT-800 0.80 Clear	GPS QHY174M	1.0 1.0 -	V. Kashuba, N. Koshkin, V. Zhukov
Nastro Verde, Sorrento, Italy	+40.618714 +14.357628 275.0	SC Meade LX200 0.3556 Clear	NTP ASI 120 MM-S	2.5264 2.96 -3.2	Nello Ruocco
- Agerola, Italy	+40.6260833 +14.571555 708.0	SC C14 EDGE HD 0.355 Clear	NTP ASI 178 mono	0.6 0.6 -	Luigi Morrone
Algiers-Bouzareah, Algiers, Algeria	+36.79787333 +03.032248333 348.3	Ritchey-Chretien 0.81 Clear	GPS WATEC 910 HX/RC	0.08 0.08 -0.04	D. Baba Aissa, Z. Gringhacene
Roque de Los Muchachos, La Palma, Spain	+28.7624 -17.8792 2363.0	Liverpool 2.0 V+R	NTP Andor DW485 (RISE)	0.6 0.6324 -	Pablo Santos-Sanz Nicolás Morales, José Luis Ortiz
EPTOs, Tijarafe, Spain	+28.741667 -17.92972223 1079.0	Marcon RC 0.40 Clear	NTP FLI PL4240	4.0 5.0 +1.0	Daniele Carosati
Astronomic Society of Tunisia, Ariana, Tunisia	+36.8842 +10.1949 5.0	- 0.203 Clear	GPS ZWO ASI 120 MM	2.0 2.0 -1.894	Sofien Kamoun
Teide, Spain	+28.3000 -16.5097 2390.0	Artemis 1.0 Clear	GPS Andor IKONL BEX2 DD	1.5 2.0 -	Artem Burdanov, Julien de Wit
Teide, Spain	+28.3000 -16.5097 2390.0	TAR1 0.46 Clear	NTP FLI KL 400	1.0 1.0 -0.5	Miquel Serra-Ricart, Miguel R. Alarcón, Javier Licandro
Serra La Nave, Catania, Italy	+37.69291 +14.97355 1727.0	- 0.91 Clear	NTP Developed at observatory	6.0 10.0 +2.0	A. Frasca, G. Catanzaro, R. Zanchez, Giuseppe Leto
Kuban State University, Kuban, Russia	+45.01667 +39.0333 76.0	Paramount ME 0.508 Luminance	GPS FLI PL1001E	3.0 5.0 -	A.L. Ivanov, V.A. Ivanov, N.B. Ivanova
Istanbul University, Çanakkale, Turkey	+40.09899 +26.47449 410.0	İST60 0.6 Clear	GPS Andor iXon Ultra 888	2.0 3.0 -	Süleyman Fişek, Oğuzhan Çakır, Simge Özer

Table B.2: Observational circumstances of all the stations that acquired data of the 8 August 2020 event but did not detect the occultation. The symbol * indicates that this information is from the observatory website .

Observatory, nearest city, country	Latitude (°), longitude (°), altitude (m)	Telescope, aperture (m), filter	Time source, instrument	Exposure (s), cycle (s)	Observers
Sternwarte Comthurey, Neustrelitz, Germany	+53.26608 +13.1901666 74.0	- 0.18 Clear	GPS QHY174	2.964 2.964	Konrad Guhl
Breitenweg, Herkenrath, Germany	+50.993310 +07.183794 200.0	RC 0.304 Clear	GPS Watec 120N+	2.56 2.56	Bernd Klemt
Biesenthal, Biesenthal, Germany	+52.759278 +13.663 263.0	Newtonian 0.3 Clear	GPS QHY174	0.6 0.6	Nikolai Wüensche
- Berlin, Germany	+52.516111 +13.427778 40.0	Newtonian 0.254 Clear	GPS DVTI	3.0 3.0	Christian Weber
Éppstein-Bremthal, Wiesbaden, Germany	+50.13816667 +08.364 256.0	Schmidt-Cassegrain 0.254 Clear	GPS QHY-174M	3.0 3.0	Oliver Klös
Vierzon, Vierzon, France	+47.223258 +02.052731 100.0	Newtonian 0.25 Clear	Time Box ZWO 1600 M	1.5 1.5	Lionel Rousselot
Borowiec, Poznan, Poland	+52.276896 +17.075216 123.0	Newtonian 0.4 Clear	NTP SBIG ST7	3.0 5.0	Anna Marciniak
Teplice, Teplice, Czech Republic	+50.63833 +13.84675 275.0	Planewave CDK17 0.43 Clear	TimeBox Apogee Aspen CG9000	0.5 0.58	Zdenek Moravec
Plzen, Plzen, Czech Republic	+49.69475 +13.321 339.0	- 0.303 Clear	GPS QHY 174	1.0 -	Jiri Polak
Plzen, Plzen, Czech Republic	+49.7073333 +13.3321667 326.0	- 0.303 Clear	GPS QHY 174	1.0 -	Michal Rottenborn
Ksiezyno, Bialystok, Poland	+53.075944 +23.102194 145.0	Newtonian 0.3 Clear	GPS QHY174	2.0 -	Wojciech Burzynski, Maciej Borkowski
Ondrejov, Ondrejov, Czech Republic	+49.91056 +14.78364 528.0	- 0.65 Clear	NTP Moravian G2-3200	6.0 -	Kamil Hornoch
Allariz, Orense, Spain	+42.2 -07.77 490.0	- 0.254 Clear	NTP QHY6	8.0 ≈10.0	Luis Perez
Buelach, Buelach, Switzerland	+47.51956 +08.57064 550.0	Newtonian 0.50 Clear	GPS DVTI	0.2 0.2	Stefan Meister
MPI für extraterrestrische Physik, Garching, Germany	+48.261388889 +11.671111111 480.0	- 0.61 Clear	GPS SBIG STX-16803	3.0 12.9	Vadim Burwitz, Piotr Sybilski, Wienczyslaw Bykowski, Thomas Müller
Giesing, Munich, Germany	+48.12194 +11.6072 500.0	Cassegrain 0.80 Orange	Computer Atik 3141	1.355 1.355	Bernd Gährken
Český Rudolec - Matějovec, Strmilov, Czechia	+49.08277778 +15.22841667 707.0	- 0.203 Clear	GPS QHY 174M	2.5 -	Jiří Kubánek
Wendelstein, Brannenburg, Germany	+47.703638889 +12.012055556 1836.0	- 2.1 SDSS r + SDSS i	GPS 3kk	1.0 13.0	Michael Schmidt, Ulrich Hopp
Nonndorf, Waidhofen an der Thaya, Austria	+48.78695667 +15.23565667 549.0	- 0.254 Clear	GPS WAT-610BD	1.28 -	Gerhard Dangel
Cannet, Risclé, France	+43.62093 -0.044685 180.0	- 0.40 Clear	GPS Watec 120N+	1.28 -	Jean Jaques Castellani
Saint-Caprais, Rabastens, France	+43.874044 +01.718749 193.0	- 0.94 Clear	GPS WATEC 910HX	0.64 -	Eric Frappa, Alain Klotz, Maylis Lavayssiere
Zákopčie, Čadca, Slovakia	+49.4042222 +18.7026306 680.2	Newtonian 0.4 Clear	GPS QHY 5 III 290M	0.9945 0.9945	Peter Delinčák
- Muzzano-Lugano, Switzerland	+45.9862778 +08.91958333 350.0	Schmidt-Cassegrain 0.23 Clear	GPS Watec 910/HX-RC	1.28 -	Alberto Ossola

Table B.2 continued

Schiaparelli, Varese, Italy	+45.86778 +08.77083 1230.0	Reflector 0.84 Clear	NTP SBIG STX-16803	4.0 7.0	Luca Buzzi
-	+49.307305556	-			
Kysucké Nové Mesto, Slovakia	+18.765388889 469.0	0.252 Clear	GPS QHY174	380 380	Marian Urbaník
Belesta, Toulouse, France	+43.438391949 +01.83152549 234.0	- 0.20 Clear	GPS WATEC 910HX	0.64 -	Andre Pascal
Latrape, Toulouse, France	+43.243969 +01.290111 350.0	- 0.305 UV-IR block	GPS Watec 910 HX/RC	5.12 -	Michel Boutet, Jacques Sanchez
Suhora, Poreba Wielka, Poland	+49.5691728579 +20.06728579 1000.0	- 0.6 Clear	GPS Apogee Aspen-47	2.0 3.0	Waldemar Ogloza
Filzi School, Bolzano, Italy	+46.42278 +11.33833 280.0	RC Refractor 0.355 Clear	NTP ASI 294 pro	1.0 1.0	G. B. Casalnuovo
GiaGa, Pogliano Milanese, Italy	+45.54145833 +08.9954750 172.0	Schmidt-Cassegrain 0.356 Clear	NTP Moravian G2-3200 Mark II	4.0 12.33	Galli Gianni
Škalnaté Pleso, Tatranská Lomnica, Slovakia	+49.189355 +20.233816 1786.0	- 0.61 Clear	NTP SBIG ST-10XME	4.0 6.8 -	Marek Husárik
Škalnaté Pleso, Tatranská Lomnica, Slovakia	+49.1894 +20.2341 1786.0	- 1.3 Clear	NTP ZWO ASI 1600MM pro	1.0 1.0	Richard Komžík, Theodor Pribulla, Dusan Tomko
Chante-Perdrix, Dauban, France	+43.99972222 +05.6475 630.0	SC 0.275 Clear	NTP SBIG ST8-XME	2.0 4.1	Marc Serrau, X. Delmotte
Centro de Ciência Viva, Constância, Portugal	+39.49489 -08.32367 147.0	RC 0.508 Clear	GPS WATEC 910HX-RC	0.64 0.64	Rui Gonçalves, João Ferreira, Maximo Ferreira, Miguel Bento
Cima Ekar, Asiago, Italy	+45.8494453 +11.5688257 1369.9	- 0.67 Clear	NTP Moravian G4-16000	4.0 -	Domenico Nardiello
Montsec, Catalonia, Spain	+42.051666 +0.7297222 1570	Joan Oró 0.8 V	NTP+GPS* MEIA3	5.0 ≈8.85	Toni Santana-Ros
TURKSAT, Ankara, Turkey	+39.636632 +32.804157 950.0	TURKSAT 0.5 Clear	GPS FLI PL4240	3.0 5.0	Mehmed Naim Bagiran
TÜBİTAK National Observatory, Antalya, Turkey	+36.825271 +30.3333 2500.0	T100 1.0 Clear	GPS SI 1100	3.0 6.45	Yucel Kilic, Orhan Erece, Sila Eryilmaz
Çukurova University, Adana, Turkey	+37.059684 +35.3554 130.0	Pro RC 500 LK7 0.50 Clear	NTP Apogee Aspen CG6	5.0 5.0	Mahmut Tekeş
Adiyaman University, Adiyaman, Turkey	+37.751667 +38.225278 675.0	ADYU60 0.61 Clear	GPS Andor iKon-M 934	3.0 3.0	Eda Sonbas, Huseyin ER

Table B.3: Observational circumstances of all the sites that attempted to observe the 8 August 2020 event, but experienced bad weather or technical issues and did not acquire any data.

Observatory, nearest city, country	Latitude (°), longitude (°), altitude (m)	Telescope aperture (m) filter	Time source, instrument	Observers
Pinsoro, Pinsoro, Spain	+42.19916666 -01.33888888 365.0	- 0.28 Clear	GPS Mintron MTV-12V6HC-EX	Oscar Canales Moreno
Montseny, Sant Celoni, Spain	+41.7214 +02.5206 300.0	- 0.254 Clear	NTP ST8	Josep M. Trigo-Rodríguez
Sabadell, Sabadell, Spain	+41.55002777 +2.08333333 224.0	- 0.5 Clear	GPS Watec 910HX-RC	Carlos Perelló
Calar Alto, Almería, Spain	+37.22083245 -2.540997836 2168.0	- 1.23 Clear	NTP PlanetCam	Ricardo Hueso, A. Sánchez-Lavega
Urseanu, Bucharest, Romania	+44.448611 +26.093056 100.0	- 0.405 Clear	NTP ZWO ASI 224 MC color	Mihai Dascalu
Traian - Ialomița, Slobozia, Romania	+44.761488 +27.341830 30.0	Newtonian 0.2 UV/IR Cut	NTP QHY 163 M	Daniel Nicolae Bertesteanu
- - Romania	- - -	- 0.2 -	- ASI1600	Vlad Dumitrescu Bogdan Dumitru
TRAPPIST-North, Oukaimeden, Morroco	+31.2061 -7.8664 2751	- 0.6 Clear	NTP Andor IKONL BEX2 DD	Emmanuel Jehin
AGM, Marrakech, Morroco	+31.173411 -8.077456 400.0	- 0.355 Clear	NTP DMK 31AU03.AS	Mohammed Sabil
Specca, Ioannina, Greece	+39.60175 +20.87014 480.0	- 0.2 Clear	GPS Canon Eos 1200D	Georgios Lekkas
Empesos, Agrinion, Greece	+39.02570544 +21.31730396 334.0	- 0.25 Clear	Occult Flash Tag ZWO ASI 224 MC	Vagelis Tsamis, Kyriaki Tigani
- Amfiloxia, Greece	+38.805170 +21.173370 218.0	- 0.25 Clear	NTP ATIK 460exm	Nick Sioulas
Istanbul Univ., Istanbul, Turkey	+41.011749 +28.965718 60.0	İST40 0.4 Clear	NTP Moravian G2 8300	Süleyman Fişek, Oğuzhan Çakır
Univ. of Athens Observatory - UOAO, Zografos, Greece	+37.968561 +23.783368 250.0	Cassegrain 0.4 Clear	NTP ZWO ASI 290MM	Kosmas Gazeas
Eskisehir Univ., Eskisehir, Turkey	+39.885472 +30.460689 1005.0	- 0.4 Clear	GPS FLI	Metin Altan
Ondokuz Mayıs Univ. Samsun, Turkey	+41.367727 +36.201576 150.0	- 0.37 Clear	GPS SBIG STL-4020M	Selami Kalkan

Table B.4: Observational circumstances of all stations that detected 2002 MS₄ in a stellar occultation on the other eight events.

Date	Site/country (detection)	Latitude (° ' ") longitude (° ' ") altitude (m)	Telescope aperture (m) filter	Time source instrument	Exposure (s) cycle (s) correction (s)	Observers
09 July 2019	San Pedro de Atacama/CHL	22 57 11.4 S 68 10 47.6 W 2,396.9	OPSPA 0.4 Luminance	NTP Proline PL16803	2.0 ≈ 3.67	Alain Maury, Joaquín Fábrega Polleri
		22 57 12.1 S 68 10 46.8 W 2,398.5	ASH2 0.407 Clear	NTP SBIG STL11000	8.0 ≈ 10.5	Nicolás Morales
	Pico dos Dias/BRA	22 32 07.8 S 45 34 57.5 W 1,810.7	Perkin-Elmer 1.60 -	GPS Andor Ixon 4269	0.3 ≈ 1.65	Flavia L. Rommel, Rodrigo Bouffleur
26 July 2019	San Pedro de Atacama/CHL	22 57 11.4 S 68 10 47.6 W 2,396.9	OPSPA 0.4 Luminance	NTP Proline PL16803	30.0 ≈ 31.9	Alain Maury, Joaquín Fábrega Polleri
		22 57 12.1 S 68 10 46.8 W 2,398.5	ASH2 0.407 -	NTP SBIG STL11000	25.0 ≈ 27.6 +3.0	Nicolás Morales
	Paranal/CHL	24 36 57.9 S 70 23 26.0 W 2,479.2	SPECULOOS 1.0 -	- Andor Tech	2.0 ≈ 4.0	Emmanuel Jehin
	Pico dos Dias/BRA	22 32 07.78 S 45 34 57.5 W 1,810.7	Perkin-Elmer 1.60 -	GPS Andor Ixon 4269	0.8 ≈ 0.813	Gustavo Benedetti Rossi
26 July 2019	Osoyoos/CAN	49 00 31.8 N 119 21 46.7 W 1,088.0	Cassegrain 0.3 no filter	GPS QHY174M	2.0 2.0	Peter Ceravolo
19 August 2019	Penticton/CAN	49 32 02.0 N 119 33 27.0 W 0.0	Meade SCT 0.4 -	GPS QHY174M	2.5 2.5	Bruce Gowe
	Osoyoos/CAN	49 00 31.8 N 119 21 46.7 W 1,088.0	Cassegrain 0.3 no filter	GPS QHY174M	4.0 4.0	Peter Ceravolo
26 July 2020	Pretoria/ZAF	25 53 00.0 S 28 09 00.0 E 1,489.0	Celestron SCT 0.356 -	NTP ZWOASI290MM	1.0 1.015	Clyde Foster
	Johannesburg/ZAF	26 06 20.0 S 27 57 03.0 E 1,547.0	- 0.305 -	NTP ZWOASI290MM	2.0 2.015	Cory Schmitz
24 February 2021	San Pedro de Atacama/CHL	22 57 11.4 S 68 10 47.6 W 2,396.9	OPSPA 0.4 Luminance	GPS ZWO ASI6200MM Pro	10.0 ≈ 11.7	Alain Maury, Joaquín Fábrega Polleri
		22 57 12.1 S 68 10 46.8 W 2,398.5	ASH2 0.407 -	NTP SBIG STL11000	10.0 ≈ 12.8	Nicolás Morales
14 October 2021	Osoyoos/CAN	49 00 32.1906 N 119 21 46.268 W 0.0	Celestron SCT 0.35 no filter	GPS QHY174M	3.0 3.0	Peter Ceravolo
	Flagstaff/USA	35 12 10.4508 N 111 40 01.416 W 2216.0	Ritchey–Chrétien 0.318 -	GPS CMOS	2.498 2.4996	Michael Collins
10 June 2022	La Palma/ESP	28 45 45.0576 N 17 52 45.12 W 2,387.63	Liverpool 2.0 -	NTP Andor DW485 (RISE)	1.183 1.2226	René Duffard, Jose Luis Ortiz, Nicolás Morales Pablo Santos Sanz
	Teide/ESP	28 18 00.00 N 16 30 34.92 W 2,390.0	Artemis 1.0 Clear	GPS Andor IKONL BEX2 DD	1.0 1.81 +0.5	Emmanuel Jehin, Khalid Barkaoui, Michaël Gillon
	Tree Gate Farm/USA	33 20 51.5376 N 88 43 58.3114 W 93.05	Schmidt–Cassegrain 0.2 -	NTP Atik 414ex via Ekos	5.0 5.4518 -0.8	Jean-Francois Gout

Table B.5: Observational circumstances of all the stations that did not detect 2002 MS4 or experienced bad weather during the other eight stellar occultations. [†] This instrument is described in [Copejans et al. \(2013\)](#).

Date	Site/country (detection)	Latitude (° ' ") Longitude (° ' ") Altitude (m)	Telescope aperture (m) instrument	Exposure (s) cycle (s) time source	Observers
09 July 2019	Guaratinguetá/BRA (technical problems)	22 48 10.02 S 45 11 30.5 W 573.0	Meade LX200 0.4 Merlin Raptor	- - -	Rafael Sfair, Thamiris Santana, Othon Winter
	Ponta Grossa/BRA (negative)	25 05 22.2 S 50 05 56.4 W 909.0	Meade RC400 0.406 Merlin Raptor	1.5 1.5 GPS	Chrystian L. Pereira, Marcelo Emilio
	La Silla/CHL (bad weather)	29 15 32.1 S 70 44 01.5 W 2,375.0	NTT 3.58 SOFI	- - -	Emmanuel Jehin
	Cerro Pachón/CHL (bad weather)	30 14 16.41 S 70 44 01.11 W 2,713.0	SOAR 4.0 Merlin Raptor	- - -	Julio I. B. Camargo
	San Juan/ARG (negative)	31 47 54.7 S 69 17 44.1 W 2,552.0	CASLEO 2.15 PI-2040B	- - -	Luis A. Mammana, Eduardo F. Lajus
	Córdoba/ARG (negative)	31 21 24.58 S 64 35 34.41 W 864.0	- - -	- - -	Carlos A. Colazo
	Santa Rosa/ARG (negative)	36 38 16.0 S 64 19 28.0 W 182.0	Celestron C8-NGT 0.2 Meade DSI-I	5.0 6.0 NTP	Julio Spagnotto
	Sutherland/ZAF (bad weather)	32 22 46.8 S 20 48 36.0 E 1,810.0	SAAO 1.0 SHOC [†]	- - GPS	Amanda Sickafoose
26 July 2020	La Reunion Island/FRA (bad weather)	- - -	- - -	- - -	Jean Paul, Piere Thierry
	Santa Rosa/ARG (bad weather)	36 38 16.0 S 64 19 28.0 W 182.0	Celestron C8-NGT 0.2 QHY174M	- - GPS	Julio Spagnotto
		36 38 08.48 S 64 17 16.79 W 198.784	Skywatcher 0.2 QHY174M	- - GPS	Aldo Javier Wilberger
24 February 2021	Cerro Pachón/CHL (negative)	30 14 16.41 S 70 44 01.11 W 2,713	SOAR 4.0 Merlin Raptor	1.0 1.0 GPS	Altair Gomes Júnior, Flavia L. Rommel, Julio I. B. Camargo
14 October 2021	Columbus North Carolina/USA (Technical Problems)	35 13 32.1 N 82 09 17.6 W 326.0	Celestron Edge 0.36 ZWO ASI 1600mm	- - NTP	Randy L. Flynn
	North Carolina/USA (Cloudy)	35 37 19.8 N 82 33 59.9 W 700	Celestron EdgeHD 14" 0.356 Atik One 6.0	- - -	David Wake
	Indiana/USA (Cloudy)	41 16 15.03 N 87 22 31.08 W 195.7	RCOS 20" 0.51 FLI PLO9000	- - NTP	Adam W. Rengstorf
	Oregon/USA (Cloudy)	43 47 29.4 N 120 56 26.88 W 1920.0	- 0.61 Andor Xyla	1.0 1.0 GPS	Scott Fisher
	Alberta/CAN (Cloudy)	- - -	- - -	- - -	Phil Langill
	North Dakota/USA (Cloudy)	- - -	- - -	- - -	Sherry Fieber-Beyer
	Illinois/USA (Cloudy)	- - -	- - -	- - -	Aart Olsen
	Idaho/USA (Cloudy)	- - -	- - -	- - -	Jason W. Barnes
	Kansas/USA (Cloudy)	- - -	- - -	- - -	Greg Rudnick
	New Mexico/USA (Cloudy)	- - -	- - -	- - -	Larry Molnar
Ohio/USA (Cloudy)	- - -	- - -	- - -	Rush Swaney	
Montana/USA (Cloudy)	- - -	- - -	- - -	Bill Hanna	

Appendix C: Light curves

Here, we provide the plots of the 80 positive occultation light curves acquired during the nine events observed between 2019 and 2022. They are normalized to the unity, and the time is given in seconds, counting from 00:00:00 (UTC) of the event date. Figures C.1, C.2, C.3, C.4, and C.5 present the plots from the 8 August 2020 stellar occultation, listed from the northernmost to the southernmost stations (on each column). Figures C.6 and C.7 show the light curves from the other eight events. The black dots present the observational data and the red line is the fitted model.

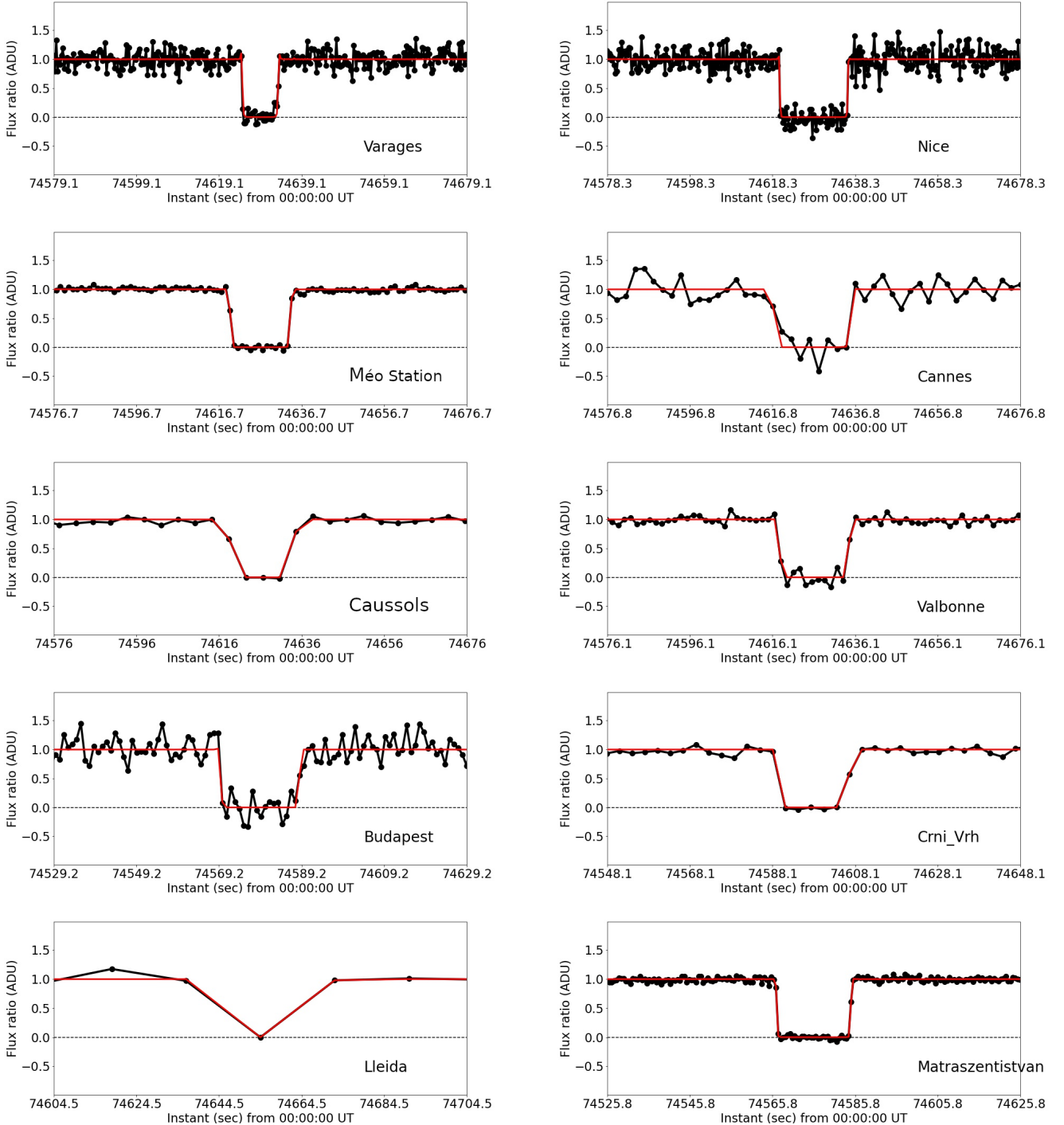


Fig. C.1: Sixty-one normalized light curves, centered in the occultation instant, obtained on the 8 August 2020 campaign. The station that acquired the light curve is mentioned in each plot. The black and red points present the observed data and the fitted model, respectively.

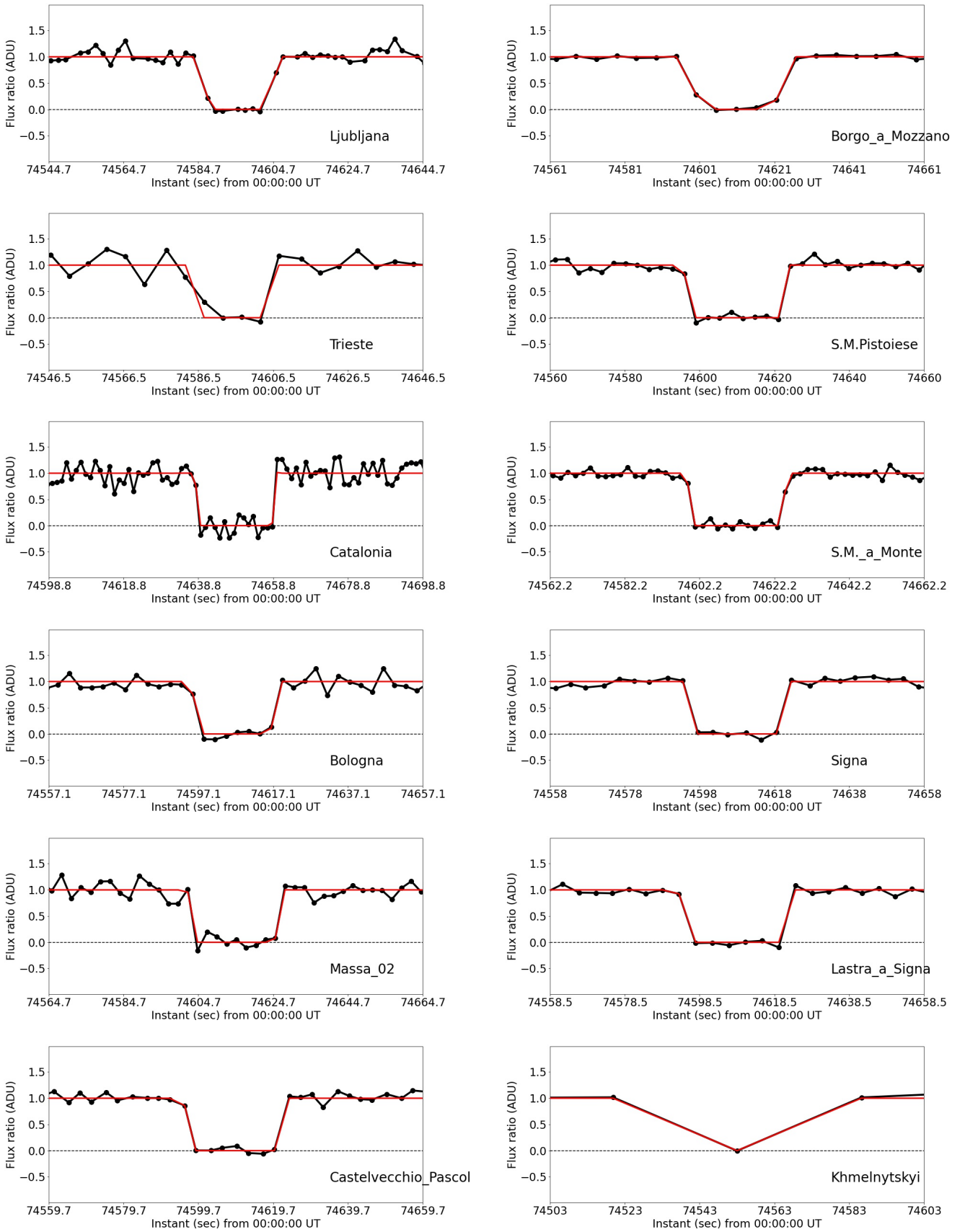


Fig. C.2: Continued.

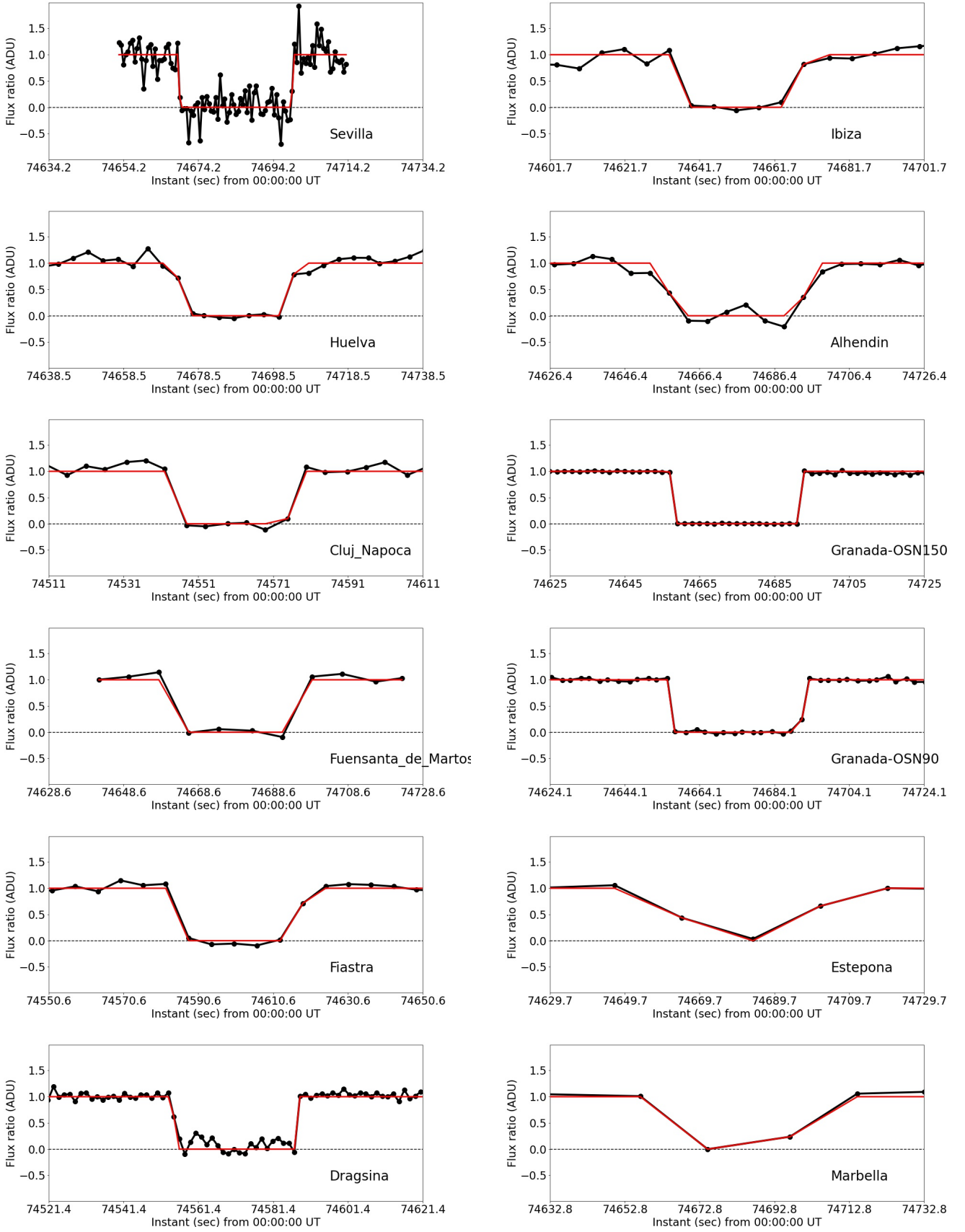


Fig. C.3: Continued.

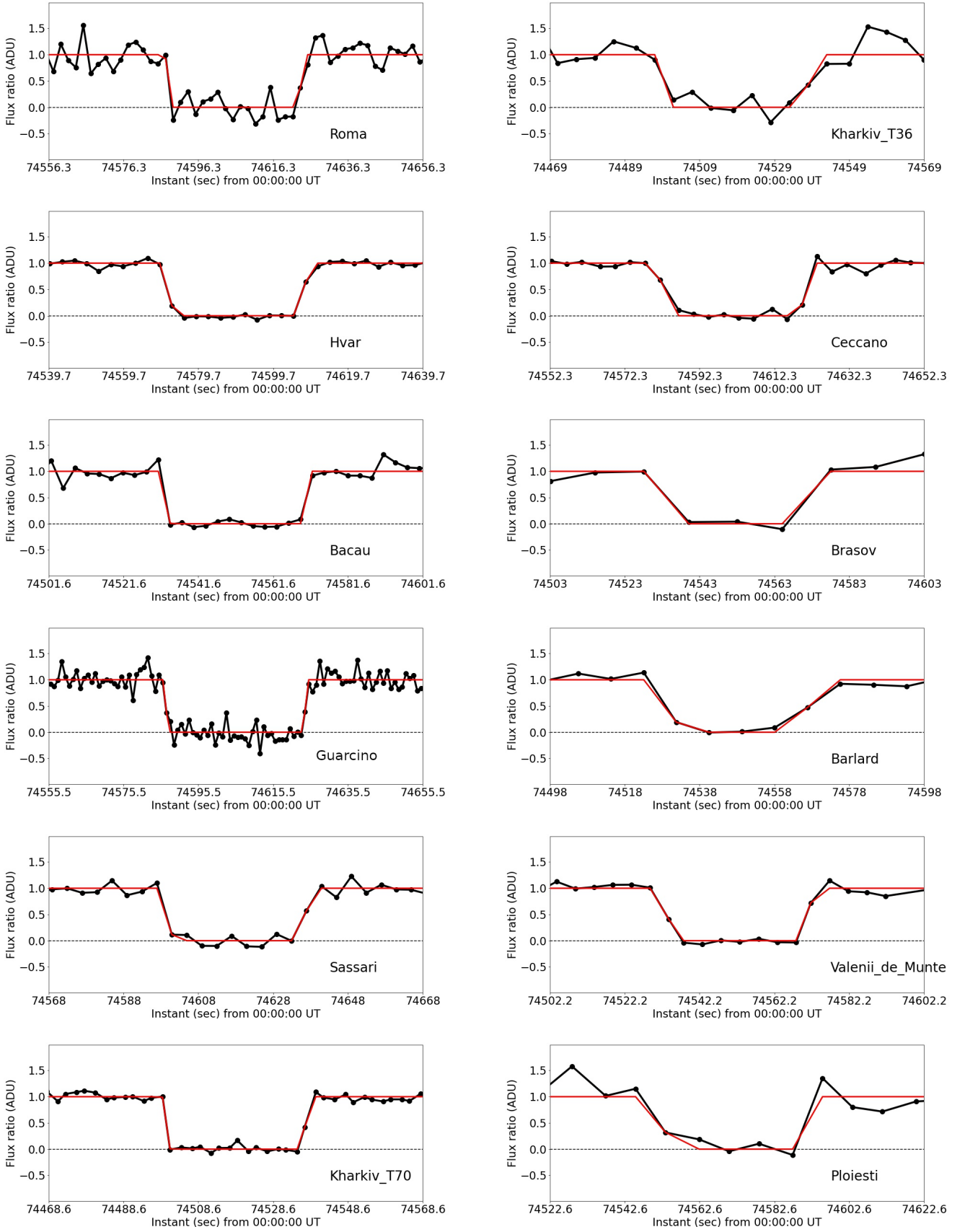


Fig. C.4: Continued.

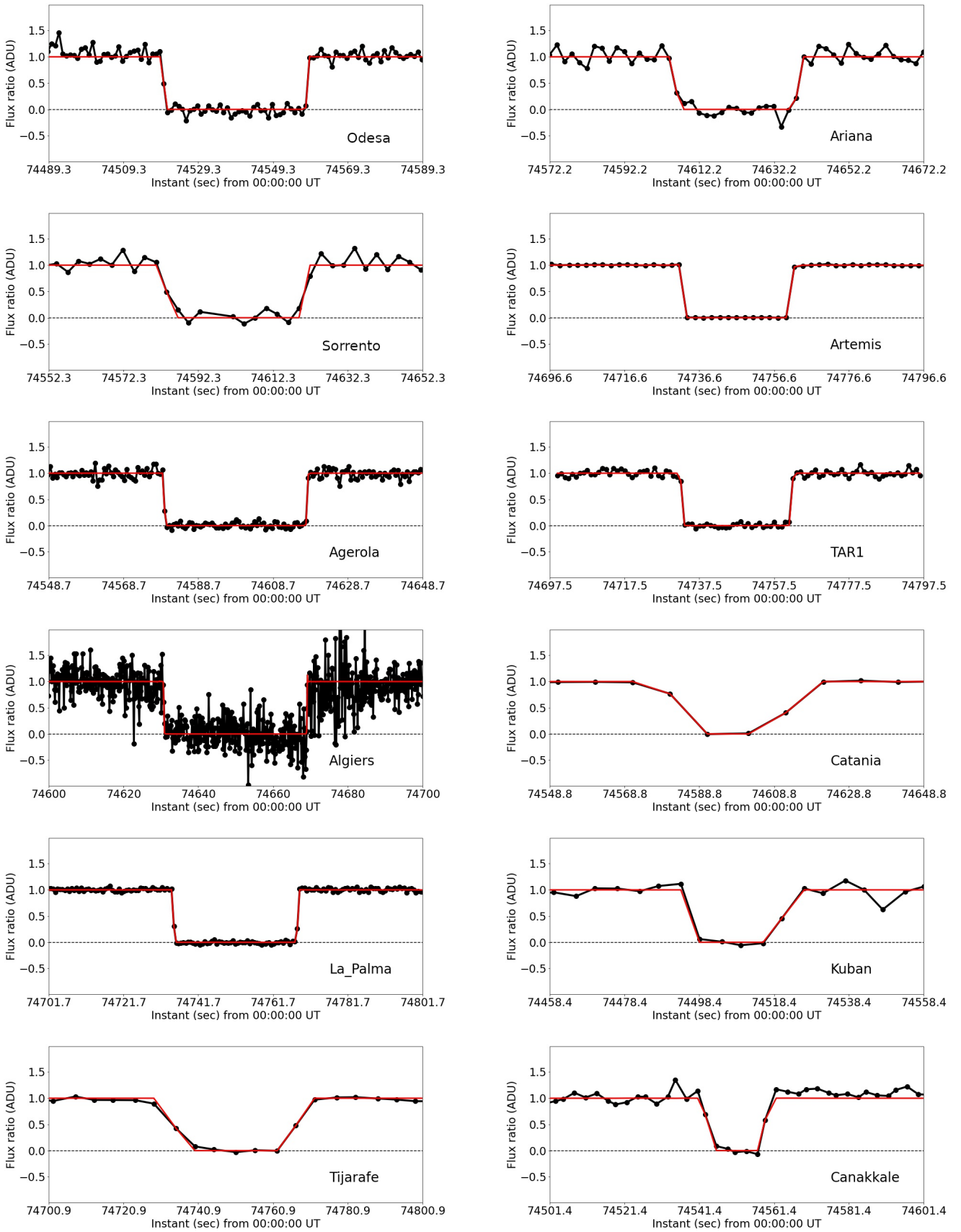


Fig. C.5: Continued.

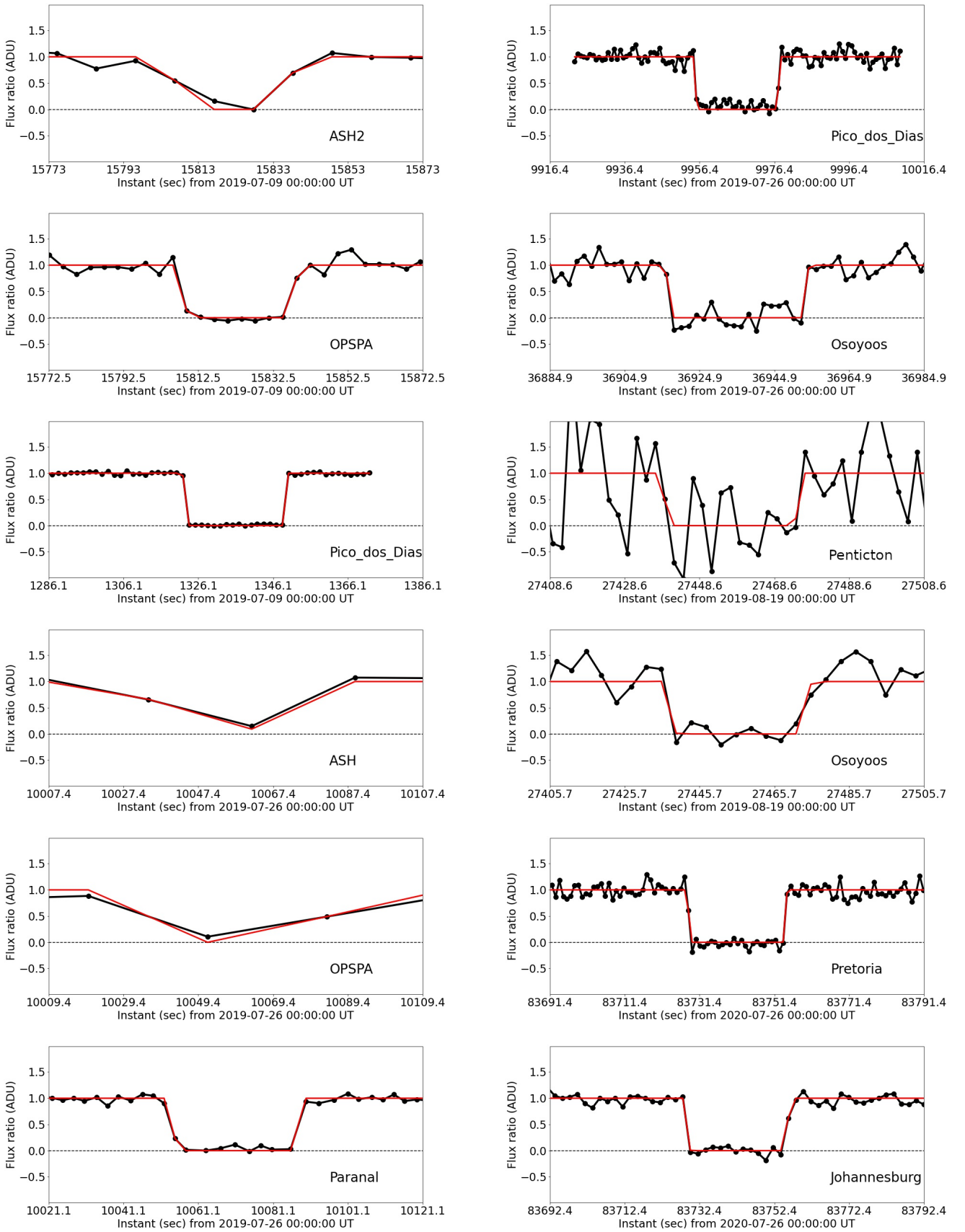


Fig. C.6: Observed (black points) and calculated (red line) light curves for each site that observed a stellar occultation by 2002 MS₄, except the 8 August 2020 multichord event. See table B.4 for observational details.

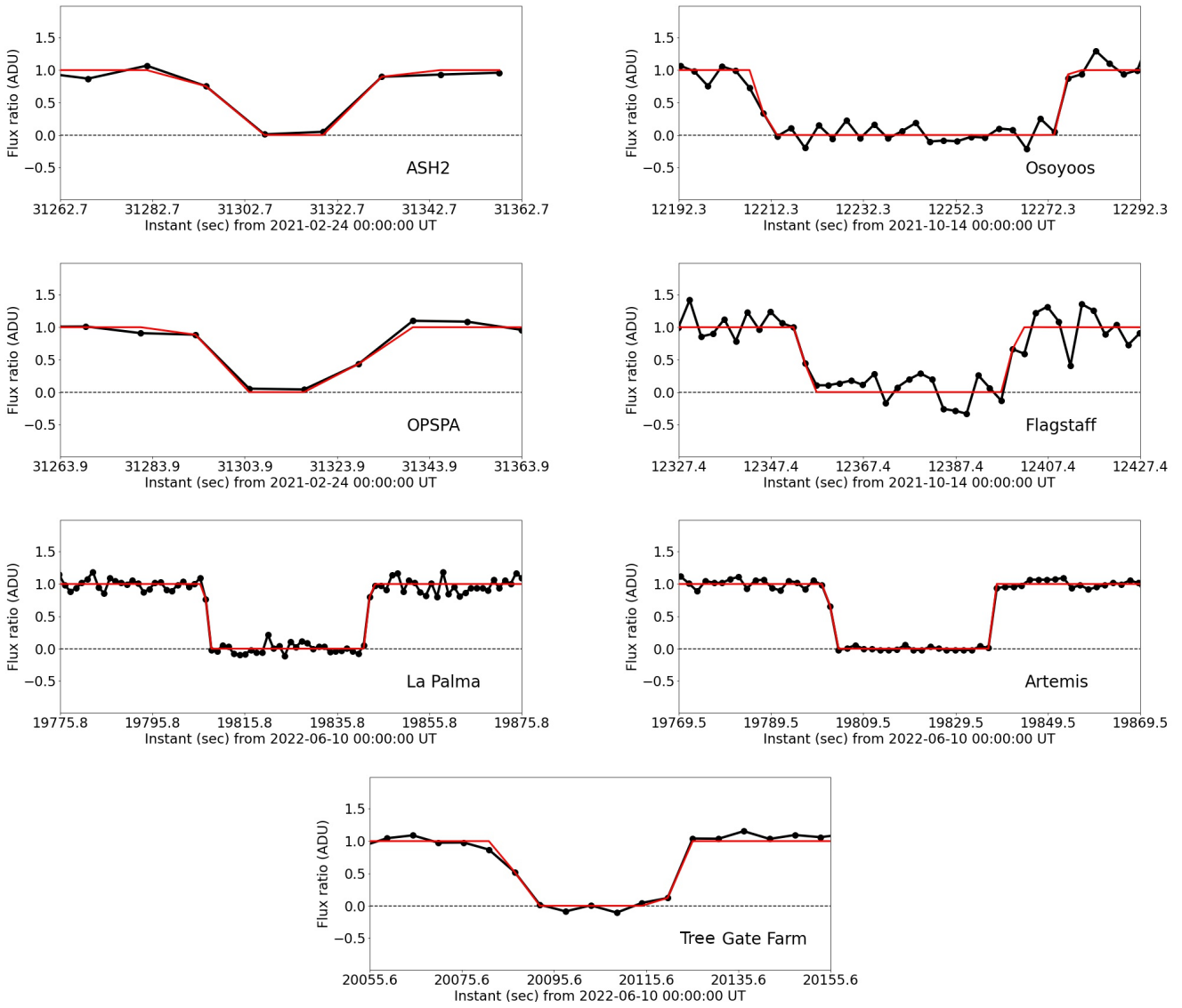


Fig. C.7: Continued.

Appendix D: The unknown satellite hypothesis

Here we present a short discussion about a hypothesis raised by the referee of a mutual event by an unknown satellite causing the ‘bulge’ on the observed limb of 2002 MS₄ during the 8 August 2020 occultation. To explore such a possibility, I used all points between 5° and 25° to fit a circular limb of the putative satellite and the points between 50° and 340° to fit the main body limb. The satellite solutions were filtered by the negative part of the Varages light curve (orange line in Fig. D.1). As a result, we derived a diameter of ≈ 788 km for the main body and ≈ 213 for the putative satellite. Considering both projected areas at the sky plane, the area’s equivalent diameter would be about 808 km. This result does not explain the diameter obtained from thermal measurements. Unless the putative satellite has a significant oblateness or if it irradiates more in the thermal than the 2002 MS₄ surface.

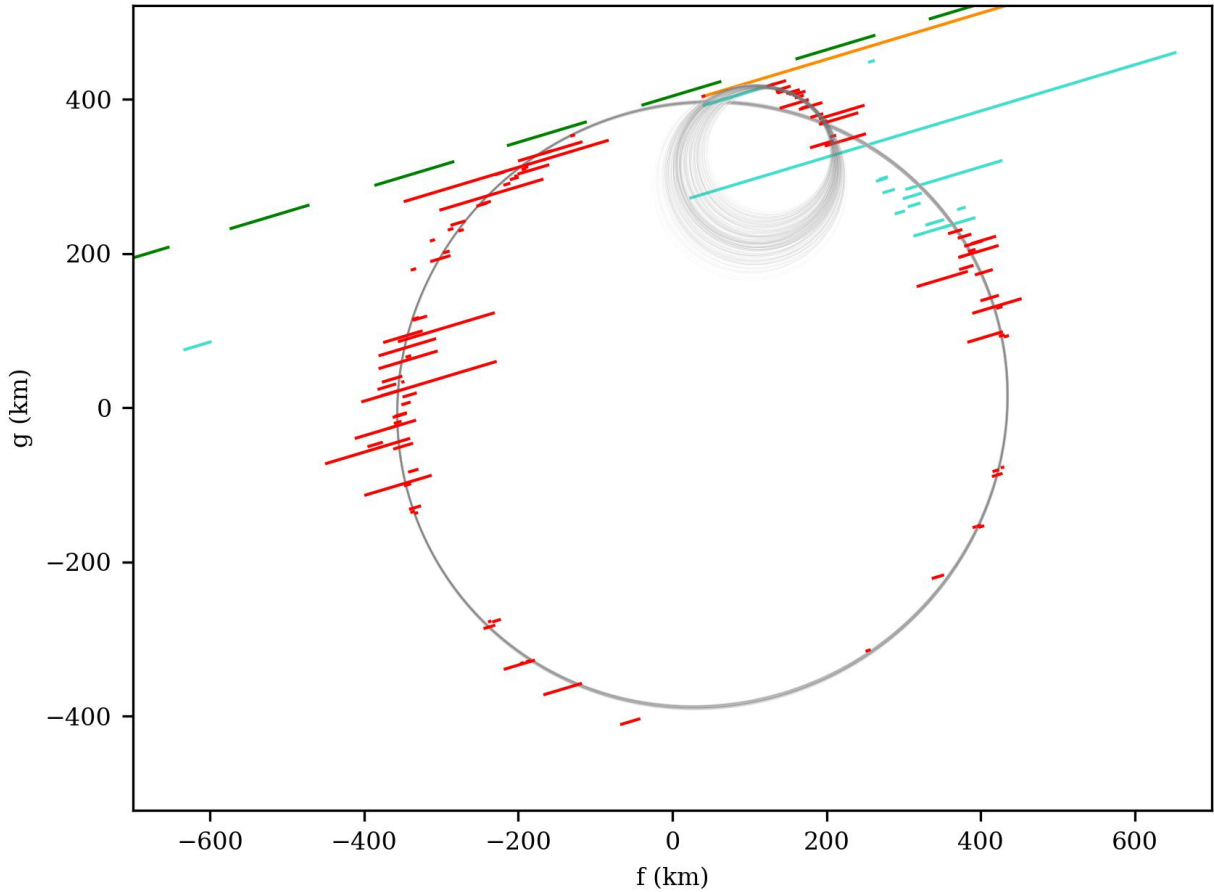


Fig. D.1: The gray regions show the 1σ fitted limb for the main body and the putative satellite. Green segments show each exposure acquired from Montsec station. This data set was the closest negative chord at North. The orange segment shows the negative part of the Varages light curve. Red segments are the observed immersion and emersion (1σ) instants used for the limb fitting. The turquoise segments are the immersion and emersion (1σ) instants not used in the fits.